Final Report
on

INVESTIGATION OF COMPRESSIBLE VORTEX FLOW CHARACTERISTICS

November 1977

CRINC-FRL 260-1

NASA Langley Research Center

NASA Contract NAS1-12976

by

Vincent U. Muirhead, Principal Investigator
Chairman, Department of Aerospace Engineering
The University of Kansas, Lawrence, Kansas 66045

Page Intentionally Left Blank

Blank

TABLE OF CONTENTS

LIST OF SYMBOLS

A	Area
M	Mach number
R	Reynold's number
a	Speed of sound
k	Constant
p	Pressure (absolute)
r	Radius
S	Speed index
v	Velocity components in plane perpendicular to axis
w	Axial velocity component
z	Axial direction
Γ	Circulation ($2\pi r_\theta$)
γ	Kinematic viscosity
ζ	Vorticity
ω	Solid body rotation

Subscripts

A	Atmospheric conditions (absolute)
o	Center of vortex core
c	Inner radius of free vortex flow
s	Static at the center line in nozzle
T	Total at the center line in nozzle
w	Z component
θ	Tangential component
Γ	Circulation
1,2	Locations along z axis

Exponents

n	Dimensional analysis exponents
m	Dimensional analysis exponents
σ	n/m

LIST OF FIGURES

Page
Intentionally
Left Blank

LIST OF TABLES

Page
Intentionally
Left Blank

SUMMARY

The objective of this investigation was to study the nature of intense air vortices and to investigate the factors which determine the intensity and rate of decay of both single and pairs of vortices. Single vortex parameters of axial pressure differential, circulation and outflow rates were varied. In addition, for dual vortices, separation distance and directions of rotation were varied.

The unconfined vortices which were generated by a single rotating cage were intensified by an increasing axial pressure gradient (increasing axial core flow). Vortex breakdown occurred when the axial gradient became negligible. The core radius was a function of the axial gradient (axial core velocity).

Dual vortices were generated by two counter-rotating cages with both large and medium cage spacing and equal cage rotation speeds. The vortices rotated opposite to the attached cages. With minimum spacing only one vortex was formed which rotated in a direction opposite to the attached cage. When one cage rotated at half the speed of the other cage, one vortex formed at the higher speed cage rotating in the cage direction.

Normally only one vortex formed with corotating cages, and the vortex rotated in the direction of the rotation of the cages. With large spacing of the cages the vortex was cyclic with unequal differential pressures applied to the cages. This

was enhanced by unequal cage speeds.

Vortices formed by counter-rotating cages were generally weaker than those formed by corotation.

1. INTRODUCTION

The objective of this investigation was to study the nature of intense air vortices and to investigate the factors which determine the intensity and the rate of decay of both single and pairs of vortices.

Various experimental approaches have been used to study vortex characteristics. Patterson[1] studied the attenuation of wing-tip vortices in the Langley Research Center towing basin. Lezus[2] conducted similar tests in the underwater towing facility at Ames Research Center. The attenuation of vortices by aircraft in flight were investigated by Tomback[3], Chavalier[4] and others. Wind tunnel studies have been conducted by Orloff and Grant[5] and numerous others. The characteristics of a single vortex have been investigated by Muirhead[6]. The latter study approached the problem from a somewhat different point of view to examine the basic vortex flow and the parameters which directly affect this flow.

During a systematic study of tornado damage by Eagleman and Muirhead[7], it became evident that damage observed was not caused by simple rotational and translational air flow. A core flow or deficit flow had to provide a major contribution to cause the destructive effect observed. Since velocity can also be thought of in terms of the pressure, a local speed index[6] of the vortex, S, was defined as

$$S = (1 - p_o/p_A)\ 1000 \qquad (1)$$

Thus, the vortex intensity at any point along the vortex axis is a function of the pressure at the center of the core at that point. The pressure at this point must be compatible with the pressure gradient along the core axis and the tangential velocities of the vortex in the plane perpendicular to the axis at this point. Since $p_o/p_A = f(\rho,\Gamma,W_o,\mu,a)$, from dimensional analysis:

$$S = (1 - \frac{k}{R_\Gamma^m M_{w_o}^n}) 1000 \qquad (2)$$

where

$$R_\Gamma = \frac{\Gamma}{\nu} \text{ and } M_{w_o} = \frac{w}{a_A}$$

The change of properties along the axis of the vortex were found by differentiation of p_o/p_A along the axis.

$$\frac{dp_o}{dz} = p_o \left[\frac{1}{p_A}\frac{dp_A}{dz} + \frac{m}{\nu}\frac{d\nu}{dz} - \frac{m}{\Gamma}\frac{d\Gamma}{dz} - \frac{n}{M_{w_o}}\frac{dM_{w_o}}{dz}\right]$$

Assuming $\frac{dp_A}{dz}$, $\frac{d\nu}{dz}$ and $\frac{da_A}{dz}$ are negligible and $\Gamma = 2\pi a_A r_c M_{\theta_c}$

$$\frac{dp_o}{dz} = p_o \left[-\frac{m}{r_c}\frac{dr_c}{dz} - \frac{m}{M_{\theta_c}}\frac{dM_{\theta_c}}{dz} - \frac{n}{M_{w_o}}\frac{dM_{o_w}}{dz}\right]$$

and

$$\frac{dr_c}{r_c} = -\frac{1}{m}\frac{dp_o}{p_o} - \frac{dM_{\theta_c}}{M_{\theta_c}} - \frac{n}{m}\frac{dM_{w_o}}{M_{w_o}}$$

integrating

$$r_{c_2} = r_{c_1}\left[\left(\frac{p_{o_1}}{p_{o_2}}\right)^m \left(\frac{M_{\theta_{c_1}}}{M_{\theta_{c_2}}}\right) \left(\frac{M_{w_{o_1}}}{M_{w_{o_2}}}\right)^{\frac{n}{m}}\right]$$

$$r_{c_2} = r_{c_1} \left[\left(\frac{p_{o_1}}{p_{o_2}}\right)^m \left(\frac{v_{\theta_{c_1}}}{v_{\theta_{c_2}}}\right) \left(\frac{w_{o_1}}{w_{o_2}}\right)^{\frac{n}{m}}\right] \tag{3}$$

If the flow is assumed isentropic, then

$$p_{o_2} = p_{o_1} \text{ and } v_{\theta_c} = 2w_o$$

$$r_{c_2} = r_{c_1} \left[\left(\frac{w_{o_1}}{w_{o_2}}\right)^{1 + \frac{n}{m}}\right] = r_{c_1} \left[\left(\frac{w_{o_1}}{w_{o_2}}\right)^{\sigma}\right] \tag{4}$$

Equation (4) indicates that the core radius is a direct function of the center core flow velocity. As the core flow approaches zero, the core radius grows rapidly. Assuming the circulation remains constant during the growth of the core, it does diffuse the vorticity; and, because of the lack of organization for the vorticity, it facilitates the decay of the vorticity ($\Gamma = \int dA \simeq 2\omega A \sim \omega r^2$).

The core flow decay may occur by conveying turbulent energy radially[8] from the core into the free vortex flow region through the spiral vortices surrounding the core region[6], by artifically reducing the core axial flow[9], or by the interaction of one vortex with another[10]. Owen[8] suggests that turbulent energy is conveyed to the free vortex region by radial viscous diffusion over distances proportional to (time)$^{1/2}$. This suggests that σ (equation 4) is of the order of 1/2.

2. APPARATUS AND PROCEDURES

2.1 Vortex Generators

Vortices were generated by the use of two rotating wire cages, Figure 2.1.1. The cages were rotated independently by

two three-horsepower constant speed motors through belt drives. The pulley diameters were changed to obtain maximum rotating speeds of 1200 and 600 r.p.m. The direction of cage rotation was changed by reversing the motors.

The wire cages were .5842 meters in diameter and .4826 meters in axial length. In the center of the disk at the top of each cage was an outflow orifice. Three nozzles of .1016, .0762 and .0381 meters in diameter were used to vary the outflow. Three different distances were used between the cage centerlines: 2.50, 1.89 and .673 meters. The bottoms of the cages were located 2.394 meters above the floor of the test chamber. A false floor was placed .324 meters above the test chamber floor.

Suction pressures were applied to the cage nozzles. The absolute pressures varied from 5×10^3 Newtons/meter^2 to an atmospheric pressure of about 98×10^3 Newtons/meter^2. The suction pressures were provided by vacuum tanks (60 meters^3) and three vacuum pumps. The maximum suction was applied and allowed to decay to atmospheric pressure.

2.2 Instrumentation

Neutrally buoyant helium bubbles and dry ice were used to observe the vortex flow. Both photo flood lighting and xenon lighting were used in the illumination of the bubbles and dry ice. The bubble paths were recorded by either video tape or a 16mm motion picture camera. The observations with the video camera were made at two positions below the cages: .616 and 1.30 meters. Still photographs of the core were made at .432

and 2.07 meters below the cages. A voice recording was also made of the visual observations of the test director.

The static and total pressure in the cage nozzle was measured by pressure transducers and recorded, Figure 2.2.1. One Kistler piezo-electric transducer was recessed in the false floor under the cage. The cage rotational speed was obtained by use of a photo cell.

2.3 Single Vortex Procedures

The single vortex tests were conducted as indicated in Table I. A number of test runs were made for each test condition indicated. Nozzle static and total pressure, floor pressure and cage rotation speed were continuously recorded versus time. The bubble flow patterns were recorded on video tape. In addition, a few runs were recorded by a 16mm moving picture camera and still photography.

The bubble paths recorded on video tape were plotted from the tape on drafting film and xeroxed, Figure 2.3.1. These paths were digitized. The digitized data were used to calculate the velocity components of the vortex at different radii from the core. Velocity component plots were made versus radii for each bubble path plot. The rotational speed, static and total nozzle pressure were recorded on each velocity plot. By combining all of the velocity plots for a given rotational speed, static pressure and nozzle diameter, composite velocity component graphs were made. Comparisons of these component graphs were then

made to evaluate the effect of nozzle diameter, rotational speed and axial pressure gradient on the vortex strength.

2.4 Dual Vortices Procedures

The dual vortices tests were conducted as indicated in Table III. A number of tests were conducted for each test condition. Nozzle total and static pressure and cage rotation speed were recorded versus time. The bubble paths were recorded by a 16mm motion picture camera and still photography. A voice recording was made of the visual observations by the test director. These data were then evaluated to determine the effect of cage rotational speed, direction of rotation, separation distance, axial pressure and nozzle diameter on the strength of the vortices.

3. SINGLE VORTEX

3.1 Dry Ice Visualization

A dry ice visualization technique was used to obtain the photographs in Figures 3.1.1 through 3.1.8. The three basic vortex regions are shown in Figure 3.1.1 The very small diameter, low pressure, low density core flow region is surrounded by a thin region of spiral vortices. The free vortex region is shown in the low portion of the photograph surrounding the spiral vortices. This vortex was generated by steady maximum speed cage rotation and the application of maximum suction pressure at the nozzle in the center of the cage. During the tests the vortex meandered about. As the applied suction pressures decreased, the vortex meandered over a larger area. Whenever the core region came in

contact with the cage, the core flow decreased and the vortex became weaker, Figures 3.1.2 and 3.1.3. If the core was carried outside the cage and became independent of the low pressure in the center of the cage, Figure 3.1.4, the vortex became very weak. It eventually dissipated unless the core became reattached to the cage nozzle (or sink). After a vortex dissipated, a new vortex would form as in Figure 3.1.5.

Figure 3.1.6 shows a strong vortex formed by maximum steady rotation and suction pressure under the influence of a small cross air current in the laboratory. It will be noted that the vortex bends at both ends so as to approach both boundaries nearly perpendicular to the solid boundaries. The general stiffness of the strong core may also be seen.

The basic part that the axial pressure gradient plays in the vortex is illustrated by Figure 3.1.7. The cage rotation has been stopped. A strong axial pressure gradient was maintained by the high suction pressure at the cage nozzle (or sink). The vortex was sustained by the core flow transmitting energy to the free vortex through the spiral vortices. As the axial pressure gradient approached zero, the upward flow ceased and the spiral vortices unwound and dropped to the ground. The maximum axial length vortex which could be created in the laboratory (cage to floor) is shown in Figure 3.1.8. The vortex was formed using a steady cage rotation speed of 1200 r.p.m. and strong suction.

3.2 Helium Bubble Visualization

Neutrally buoyant helium bubbles were used for visualization of the vortex flow in photographs, Figures 3.2.1 through 3.2.8.

The streamlines made by the bubbles enabled a more detailed view of the vortex flow. Figure 3.2.1 shows the formation of the flow as the rotation and the axial pressure differential were being increased. The strong core flow is shown in Figure 3.2.2 of an established vortex. Figure 3.2.3 shows the surrounding free vortex flow. As the axial pressure gradient decreased, the core flow slowed and began to collect in periodic condensation regions, Figure 3.2.4. As the core flow stopped, the diameter of these periodic condensation regions enlarged and hung in mid-air, Figure 3.2.5. Rarefaction regions appeared between the condensations. The condensation regions continued to grow and began to undulate, Figure 3.2.6. The bubbles in these undulating regions then began to cluster, Figure 3.2.7. The clusters continued to grow until the final stages of breakdown occurred as in Figure 3.2.8. The vortex dispersed unless it received new energy through a new axial pressure gradient.

3.3 Core and Spiral Vortex Flow

The vortex flow was also observed from close-up by use of the helium bubbles. Figure 3.3.1 shows the flow conditions of Figures 3.1.1 and 3.2.3. The core and spiral vortex regions are surrounded by the free vortex region. A bubble is shown moving inward from the free vortex region to the spiral vortex region. The relative length of the paths of each flow can be seen during the exposure time of the photograph. The dashes visible along some particle paths were obtained by strobing the xenon light, while also using flood lighting.

Figures 3.3.2 through 3.3.12 are close-up photographs of core flow features obtained by strobed xenon lighting. In Figure 3.3.2 the foot or ground contact of the vortex core can be clearly seen. The core was very nearly perpendicular to the ground as it approached the ground. However, just slightly above the ground it made a very sharp turn and laid along the ground. In effect, a horseshoe vortex was formed. The torque of the viscous core caused it to roll over and meander over the ground. By bending over into the small horseshoe or ground leg, an opening was made to allow some air to flow into the vortex core and create an upward flow to the nozzle (or sink) in the cage.

Figures 3.3.3 and 3.3.4 show the spiral flow as the axial core flow was increasing. In Figure 3.3.3 the spiral vortices surrounding the core flow are chiefly visible. A large number of bubbles were spiraling upward around the core at about 75° angle. Figure 3.3.4 shows a close up of the several individual bubbles as they spiraled about the core. The strong, small diameter core surrounded by an intense spiral flow is shown in Figure 3.3.5. As the core flow decreased, the core and spiral vortices appeared to expand in diameter (Figure 3.3.6). The core did not expand uniformly but in regions. These regions continued to grow and form periodic regions of condensation and rarefaction, Figure 3.3.7. A breakdown of the core flow has occurred in Figure 3.3.8. A ring has appeared in the core and spiral vortex region. A close-up of the core flow near the generator is shown in Figure 3.3.9. Regions

of bubbles and regions without bubbles appear in the core region. Figure 3.3.10 shows ground region with the bubbles flowing in the core in a rather indiscriminate manner. Figures 3.3.11 and 3.3.12 show the final stages of the core breakdown just prior to the general dissipation of the vortex. Figure 3.3.11 shows several bubbles near the generator region as they undulate. Figure 3.3.12 shows the bubbles beginning to cluster near the ground.

3.4 Velocities

The single vortex test program is contained in Table I. A summary of the variation of the characteristics with the test parameters is given in Table II. Numerous tests were made under each set of test conditions. The basic bubble paths were obtained by recording the test on video tape. Sample plots obtained from the video tape are shown in Figures 2.3.1, 3.4.1 and 3.4.2. Figure 2.3.1 shows several bubble paths spiraling upward at a radius of about 12cm from the core. The bubble positions were plotted at 1/60 of a second time interval. The left core position (1) corresponded to the initial time of the spiraling bubble position. By 18/60 seconds, when the last bubble position was plotted, the core had moved to the right (18). Figure 3.4.1 shows the core flow and a close-in spiraling bubble.

In contrast to the orderly flow of Figures 2.3.1 and 3.4.1 with axial flow and pressure gradient, Figure 3.4.2 illustrates the conditions as the core began to hang as a result of lack of pressure gradient. The bubbles within the core were moving in both directions apparently under the influence of very weak local pressure gradients.

These gradients appeared to be caused by the uneven spiral vortex patterns surrounding the core as the spiral vortices degenerated into Taylor vortices.

Representative composite velocity component graphs of the single vortex flow tests are contained in Figures 3.4.3 through 3.4.9. The most significant fact established by these tests was that the vortex was extremely sensitive to changes in axial pressure gradient. These changes continually occurred due to the unsteady nature of the vortex. Although the cage rotation was steady or decreasing uniformly and the pressure at the nozzle was either steady or decreasing uniformly, the head of the core wandered about both inside and outside of the cage. Frequently the cage interferred with the core flow. As a result the effective axial pressure differential varied almost continuously. The effect of this varying axial pressure was shown in nearly every graph. This continuously varying axial pressure essentially pulsed the vortex. In order to produce more definative data on the axial pressure effects on a vortex, a larger testing facility is needed. The core flow radius must be of sufficient diameter to obtain a core flow profile. The generating cages need to be modified to force the core to remain attached to the suction nozzle.

3.4.1 Rotation without applied differential suction pressure

Figure 3.4.3 shows the variation of velocity patterns obtained with a constant cage rotation of 1200 r.p.m. No external suction pressure was applied to the nozzle. The axial pressure gradient which existed was the result of the pressure distribution in the

boundary layer of the rotating cage disk plate. The maximum differential suction pressure[11] in the boundary layer at the center of the cage disk plate was calculated to be 8.9 Newtons/meter^2. When the vortex core head was in contact with the 8.9 Newtons/meter^2 differential suction pressure, velocities increased. As the core head moved from the low pressure region, the velocities decreased. At a rotational speed of 600 r.p.m. it was frequently difficult to form a vortex. The calculated pressure differential at this speed was 2.16 Newtons/meter^2/meter.

Visible vortex breakdown occurred over a range of rotational speeds from 300 r.p.m. to less than 100 r.p.m. The vortex breakdown was apparently more dependent upon the position of the vortex relative to the low pressure region at the rotating disk than the speed of cage rotation. The minimum calculated pressure differential at breakdown was 1.08 Newtons/meter^2/meter.

3.4.2 Steady rotation with transient applied differential suction pressure.

With steady cage rotational speeds of 1200 and 600 r.p.m. differential suction pressures were applied to the nozzle in the center of the cage disk (three different nozzles were used). The applied pressure varied from 5 x 10^3 Newtons/meter^2 absolute to the atmospheric pressure of approximately 98 x 10^3 Kilo Newtons/meter^2. This pressure, p_s, was measured on the centerline in the nozzle. The total pressure, p_T, was also measured along the centerline of the nozzle.

Figure 3.4.4 shows the typical variations of the velocities

with applied suction pressures. As the axial pressure gradient increased, the core radius decreased, and the velocity components in the core, spiral vortex and free vortex regions increased. The stability of the vortex increased with the increasing of the axial pressure gradient. However, the velocities measured were essentially the same in magnitude as those in Figure 3.4.3.

When a high differential suction pressure, p_s, existed in the nozzle, a high mass inflow occurred at the nozzle. Since this high mass inflow was only partially reflected in the measured component velocities, it must be concluded that the most [illegible] mass inflow to the nozzle came along the cage disk surface in the disk boundary layer. Thus, the vortex generator did not provide the axial pressure differential to the vortex which the measured pressure in the nozzle, p_s, would indicate.

3.4.3 Decaying cage rotation with steady applied differential suction pressure

Figure 3.4.5 illustrates typical velocity profiles when the rotational speed of the cage decayed with a given value of applied differential suction pressure in the nozzle. As the cage rotation speed decreased, the core radius decreased, and the component velocities in the core, spiral vortex and free vortex regions decreased.

The core, spiral vortex and free vortex were maintained with applied differential suction pressure after the cage rotation was stopped, Figure 3.1.7. As the suction pressure decreased,

the vortex velocities decreased and the vortex eventually dissipated. This dissipation process did not go through the condensation and rarefaction and cluster stages which occurred when an applied differential suction pressure was not present.

3.4.4 Variation with location along vortex axis

Figures 3.4.6 and 3.4.7 illustrate the variation of the velocity profiles at two locations along the vortex axis. At the high position near the vortex generator, the axial and radial components of velocity are greater at all radii. The rotational velocity components are generally larger at the high position with a sharper peak occurring in the spiral vortex-region.

3.4.5 Nozzle variation

Figures 3.4.8, 3.4.4 and 3.4.9 provide a comparison of velocity profiles with nozzle area. Increasing nozzle area increased the mass flow, and it is reflected in the increasing magnitude of the axial velocity profiles. This increasing mass flow decreased the effective test time. Increased nozzle area also increased the core radius.

3.4.6 Effect of core axial velocity on radius

Equation (4) provides a relationship between the core axial velocity and the core radius. With a small axial pressure gradient and core flow (1.78 meters/sec) the core diameter was the same or less than the bubble diameter (.003 meters). When the core began to form regions of condensation and rarefaction and undulate, the core velocity was ± .019 meters/sec. and the diameter approximately .03 meters. Using these velocities and

equation (4):

$$\frac{r_{c_2}}{r_{c_1}} = \frac{1.78}{0.19}^{.5} \approx 9.7$$

which compares favorably with the measured value from photographs.

4. Dual Vortices

4.1 General

The dual vortices test program was divided into three series of tests, Table III. The three series differ only in the spacing between the vortex generators. Test series I used medium spacing, test series II used large spacing, and test series III used minimum spacing. Within each of the test series the individual tests differed by rotational speeds and directions, nozzle diameter and applied pressure level.

Figure 2.1.1 illustrates the characteristics of two counter-rotating vortices as they were formed by the rotating cages at medium spacing. As a suction pressure was applied to the nozzles (medium), Figure 4.1.1, the core velocity increased, the core diameter decreased and the spiral vortices formed between the core and the free vortices. Figure 4.1.2 shows the resultant flow with the core and tight spiral vortices. With corotation only one vortex normally was formed. Figures 4.1.3 through 4.1.6 show a single vortex formed by corotation of the cages with minimum spacing. The vortex formed with core attached to cage B. The lower portion of the vortex meandered around toward cage A, Figure 4.1.4. The upper core then became detached from the cage

sink and meandered in between the two cages, Figure 4.2.5. The core flow stopped, and the core diameter increased. The vortex was in an initial stage of breakdown. As the core attached to the sink in cage A, Figure 4.1.6, the core flow increased, the core diameter began to decrease,and the core stiffened and began to straighten under the other cage.

The general characteristics of the dual vortices formed under the influence of the above controlled parameters follow.

4.2 Core Velocities

Observed core axial velocities were cyclic and dependent upon the core head being attached to the low pressure sink at the cage disk. A sink existed at the top of each generating cage as a result of an applied differential suction pressure to the nozzle or due to radial outflow of air in the rotating plate boundary layer. When the core head was attached to the cage sink, the core outflow was evident by the bubble motion. Whenever the core head was detached from either of the two cage sinks, the core flow stopped and the bubbles defining the core hung suspended with near zero velocity.

4.3 Core Diameter

Whenever the core flow speed decreased, the core diameter increased. An increasing core velocity produced a decreasing core diameter.

4.4 Vortex Breakdown

When the tangential velocities were small with little or no axial pressure differential, the core flow stopped. Regions of

condensation of a large number of core bubbles would hang momentarily, then fall, and then ascend to the hanging state. This undulation usually continued two to three cycles before the core finally dissipated.

4.5 Core "Whipping"

Occasionally after the core flow stopped, the upper half of the hanging core would fall immediately into an eccentric, wavy shape while the bottom half remained relatively straight. Then, the wave crests whipped around the core base in circular paths. After several revolutions, either the core straightened up with the core head attaching to a cage sink with core flow resuming or the core dissipated. Occasionally, the whipping core was cyclic with the core whipping, then straightening, then whipping for several cycles before finally dissipating.

4.6 Dissipation

The dissipation of the vortices (one or two) formed by the two rotating cages was characterized by the below types of dispersion.

1. Blow-out: Blow-out occurred with an initial cessation of core axial flow, followed by a condensation and clustering of the helium bubbles defining the core, and, finally a spin-out of the core bubbles. During the spin-out, the core bubbles spiraled outward from the core axis and upward into the general vortex circulation under the influence of the residual tangential velocities.

2. Merging: The core dissolved into the general air mass

circulating about the room area. A cessation of core flow and a hanging and clustering of the core normally occurred prior to the merging or dissolving of the core.

3. Drifting: Drifting (a special case of merging) occurred following a cessation of core flow when the entire core, without any deformation, translated away from the cages to a position off the false floor. Once off the floor, the core would merge into the general air mass.

4. Inhalation: Inhalation was a form of dissipation quite unique compared to the forms above. When the vortex was terminated by inhalation, the core was sucked into one of the nozzles without a clustering of the core bubbles. Four conditions invariably preceded the inhalation: (a) hanging core, (b) mass air flow through the nozzle, (c) momentary restoration of core flow, (d) moderate to high tangential velocities.

Throughout the dissipation stage, a free vortex continued to rotate about its dispersing core while, except for those cases of inhalement, the tangential velocities slowed to almost zero just prior to the core's disappearance. When the core was inhaled, the higher axial velocities diminished just prior to the core's disappearance.

4.7 Cage rotation

Table IV contains a summary of the effect of cage rotation on the number and direction of the vortices formed.

1. Corotation

With corotation of the cages the vortices which formed

rotated in the direction of rotation of the cages. With few exceptions only one vortex existed at any one time. These vortices were strong vortices except when the vortex moved between or away from the cages. The vortices generally formed at cage A except when the spacing was a minimum. Then, there appeared to be no cage preference.

2. Counter-rotation with large and medium cage spacing.

With the counter-rotation of the cages at equal rotation speeds the vortices which formed rotated in a direction opposite to the direction of rotation of the cage to which they were attached. This occurred regardless of whether two vortices were forming simultaneously or one formed before the other. Dual vortices formed frequently.

When cage B rotated at one-half the speed of cage A, the vortices with few exceptions rotated in a direction of cage A. The vortices were attached to cage A and normally only one vortex existed at one time.

3. Counter-rotation with minimum cage spacing

With counter-rotation of the cages at equal rotation speeds the vortices which formed rotated in the direction of cage B although most of the vortices were attached to cage A. When cage B rotated one-half the speed of cage A, the vortices rotated in the direction of cage A, and only occasionally was a vortex attached to cage B. Only one vortex existed at any one time with minimum cage spacing.

In general, all vortices formed by the counter-rotating cages were weaker than those formed by corotation of the cages.

4.8 Pressure and cyclic formation

The vortex axial pressure differential varied during the tests as the vortex core moved in and out of contact with the low pressure region in the center of the cage disks. This changing pressure caused the vortices to increase and decrease in strength (decrease and increase in diameter) or pulse. When the core remained out of contact with the low pressure region the vortex dissipated.

With corotating cages and large cage spacing a distinctive phenomena of cyclic vortex formation occurred during four tests. The single vortex which formed cycled through three distinct stages and had no definite frequency of recurrence. The stages consisted of: (1) a building vortex center; (2) an established core; and (3) vortex dissipation. The primary cause of the phenomena appeared to be the unequal differential suction pressures applied to the cages. This was enhanced by unequal cage rotational speeds. However, the phenomena also occurred in one test which had equal applied pressures and equal cage rotational speeds.

5. CONCLUSIONS AND RECOMMENDATIONS

Measurements and visual observations under the research program indicated that the axial pressure gradient in a vortex significantly influences the strength of the vortex. Only a small gradient was required to maintain an axial core flow and keep the vortex organized. The following conclusions can be

drawn from the comparison of the characteristics of the single vortex and the dual vortices under the influence of the variable parameters investigated.

5.1 Single Vortex

1. The vorticity in the air generated by a cage rotation was organized into a vortex by an axial pressure gradient which produced an axial flow and spiral vortices. The spiral vortices transferred energy from the axial core flow to the surrounding free vortex region.

2. Vortex breakdown occurred when the axial pressure gradient in the vortex became negligible. The core flow stagnated into regions of condensation with regions of rarefaction in between. The regions of condensation occurred because of the small local low pressure regions produced by the spiral vortices as they transformed into Taylor vortices.

3. Once a vortex was formed it could be sustained by a strong axial pressure gradient.

4. The core radius was a function of the axial pressure differential (axial core velocity) for a given sized outflow sink area.

5. An unrestricted free air vortex was subject to very small air currents (pressure variations) and moved about in a non-periodic meandering manner.

6. Because of the meandering nature of the uninhibited vortex it was difficult to obtain quantitative data on the axial pressure gradient.

7. The vortex generators produced a small diameter core (less than .003 meters with strong core flow). This diameter was too small to investigate the core flow profile. A much larger outflow capability was needed.

5.2 Dual Vortices

1. The vortices formed by corotating cages rotated in the direction of the cage rotation. With few exceptions only one vortex existed at any one time.

2. The vortices formed by counter-rotating cages with large and medium spacing and equal rotation speeds rotated in a direction opposite to the rotation of the cages. Dual vortices formed frequently. When cage B rotated at one-half the speed of cage A, normally only one vortex existed at one time and rotated in the direction of and was attached to cage A.

3. The vortices formed by counter-rotating cages with minimum spacing and equal rotation speed rotated in the direction of cage B and were attached to cage A. When cage B rotated at one-half the speed of A, the vortices rotated in the direction of A and were nearly always attached to A. Only one vortex existed at a time with minimum spacing.

4. Vortices formed by counter-rotating cages were generally weaker than those formed by corotation.

5. Vortex breakdown occurred when the axial pressure gradient (core axial flow) was negligible.

6. With corotation and large spacing of the cages the vortex was cyclic with unequal differential suction pressures applied to the cages. This was enhanced by unequal cage rotation speeds.

5.3 Recommendations

1. The present detailed measurements and observations of vortex strength and decay phenomena have indicated that the axial pressure gradient (core flow) controlled the vortex behavior. However, the vortex generators used in this program produced a vortex core too small for detailed examination of the core velocity profile. The velocity profile of the single vortex core region should be further investigated using a vortex generator similar to the single vortex generator but capable of a much higher volume of air outflow. The outflow should be variable from 0 to approximately 35 meter^3/second. The suction pressure differential should be variable from 0 to 150 Newtons/meter^2. An axial distance of about 20 meters should be available for profile measurements.

2. The cyclic formation phenomena which occurred with the dual vortices should be further investigated. Again, this needs to be done with much larger vortex generators. This phenomena may be of interest to those in meterology as well as aerodynamics.

6. REFERENCES

1. James C. Patterson, Jr., "Lift-Induced Wing-Tip Vortex Attenuation," AIAA Paper No. 74-38, February 1974.
2. Dietrich K. Lezius, "Study of the Far Wake Vortex Field Generated by a Rectangular Airfoil in a Water Tank," AIAA Paper No. 73-682, July 1973.
3. Ivar Tomback, "Observations of Atmospheric Effects on Transport and Decay of Trailing Vortex Wakes," AIAA Paper No. 73-110, January 1973.
4. Howard Chavalier, "Flight Test Studies of the Formation and Dissipation of Trailing Vortices, J. Aircraft, Vol. 10, No. 1, January 1973.
5. K. L. Orloff and G. R. Grant, "The Application of a Scanning Laser Doppler Velocitmeter to Trailing Vortex Definition and Alleviation," AIAA Paper No. 73-680, July 1973.
6. V. U. Muirhead, "Compressible Vortex Flow," AIAA Paper No. 73-106, January 1973.
7. J. R. Eagleman and V. U. Muirhead, "Observed Damage from Tornadoes and Safest Location in Houses," Preprints, Seventh Conference on Severe Local Storms, American Meteorological Society, Boston, Mass., October 1971, pp. 171-177.
8. P. R. Owen, "The Decay of a Turbulent Trailing Vortex, The Aeronautical Quarterly, Vol. XXI, Feb. 1970, pp.69-78.

9. Joe R. Eagleman, Vincent U. Muirhead and Nicholas Willems, Thunderstorms, Tornadoes and Building Damage, Lexington Books, D. C. Heath and Company, 1975.

10. Alan J. Bilanin, Milton E. Teske and Guy G. Williamson, "Vortex Interactions and Decay in Aircraft Wakes," AIAA Journal, Vol. 15, No. 2, February 1977, pp. 250-260.

11. Hermann Schlichting, Boundary-Layer Theory, McGraw-Hill Book Co., 1968.

7. FIGURES AND TABLES

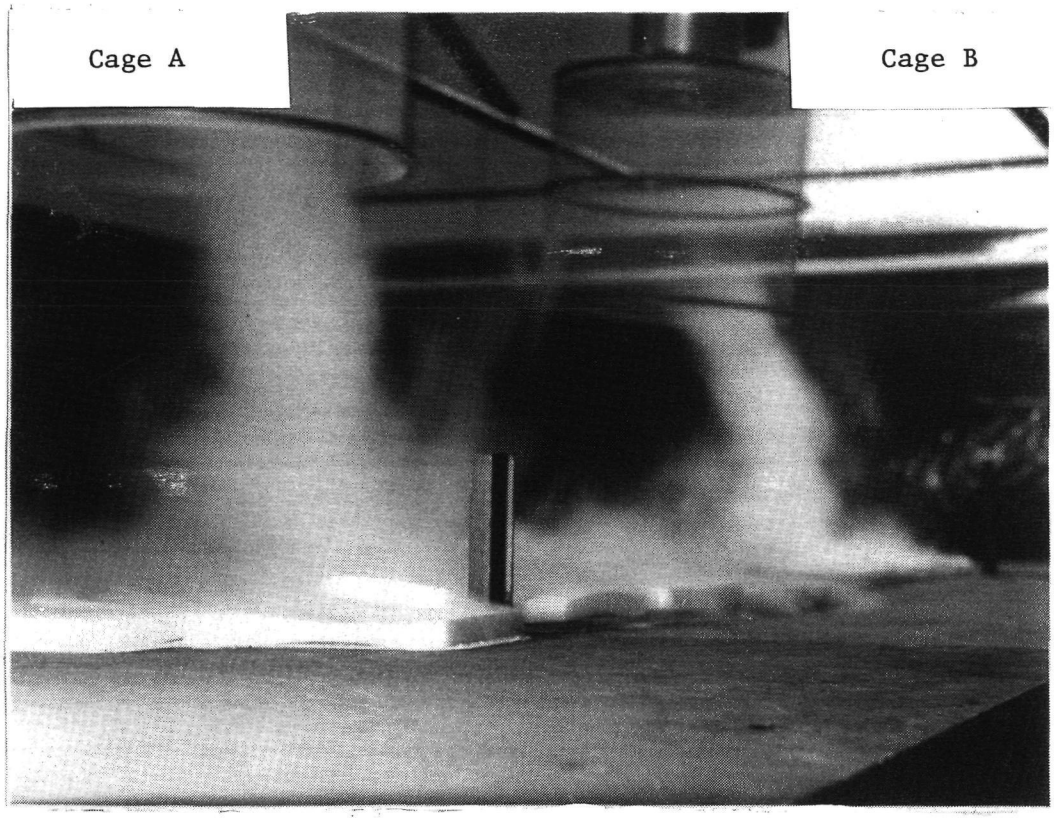

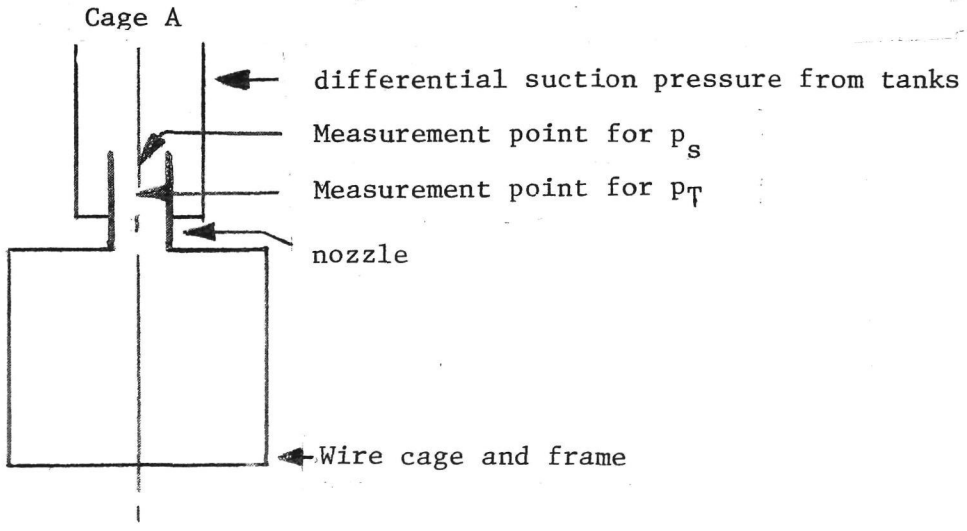

Figure 2.1.1 Dual vortices generator

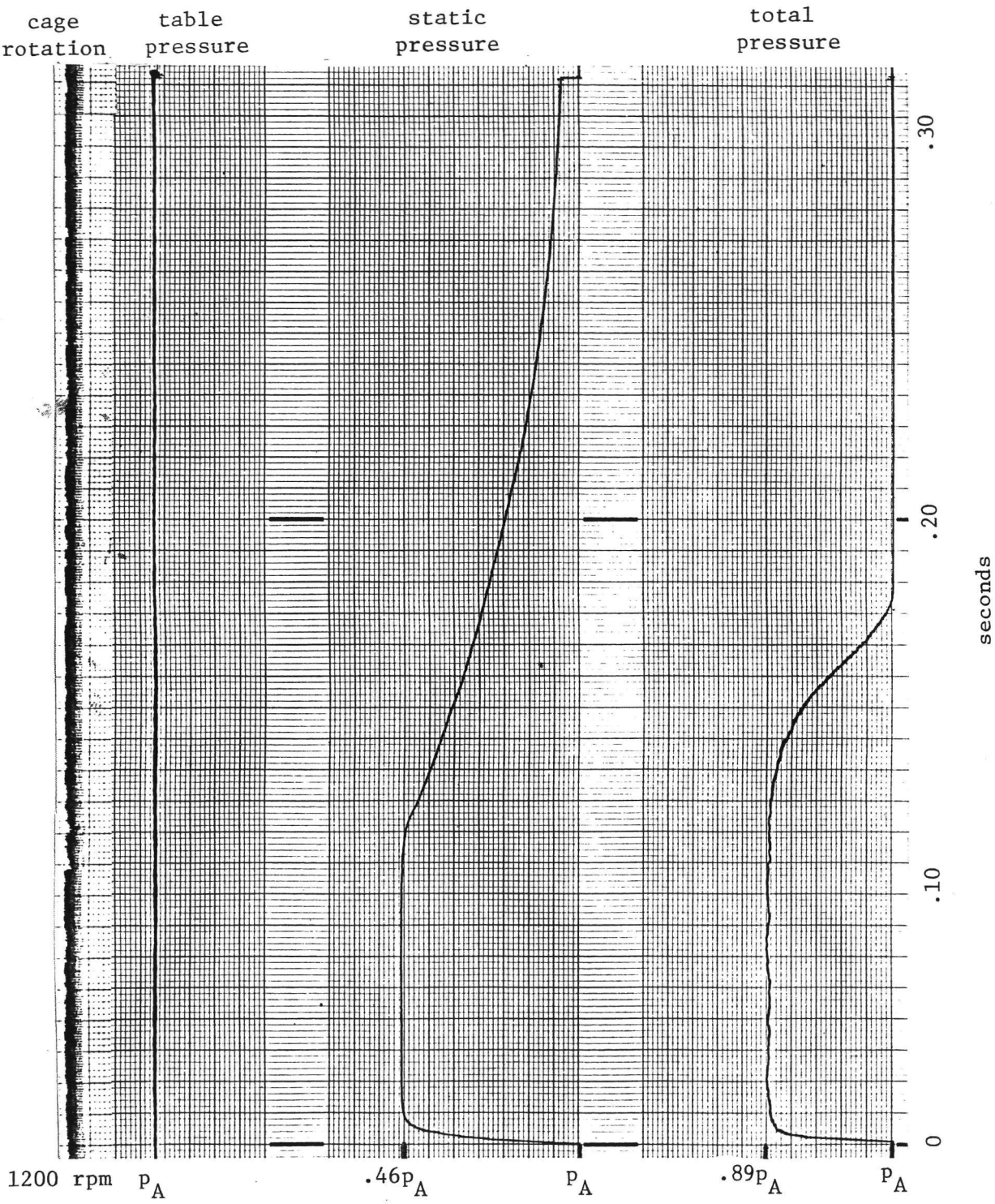

Figure 2.2.1 Pressure time record -
(dual vortices, small nozzles,
small spacing, equal pressures)

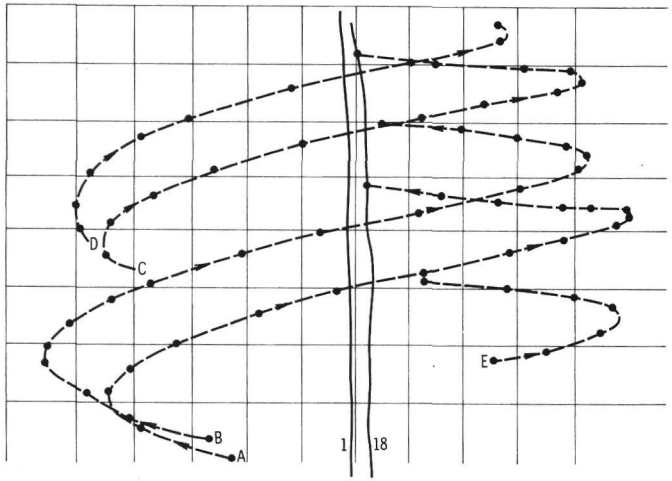

Figure 2.3.1 Bubble Paths

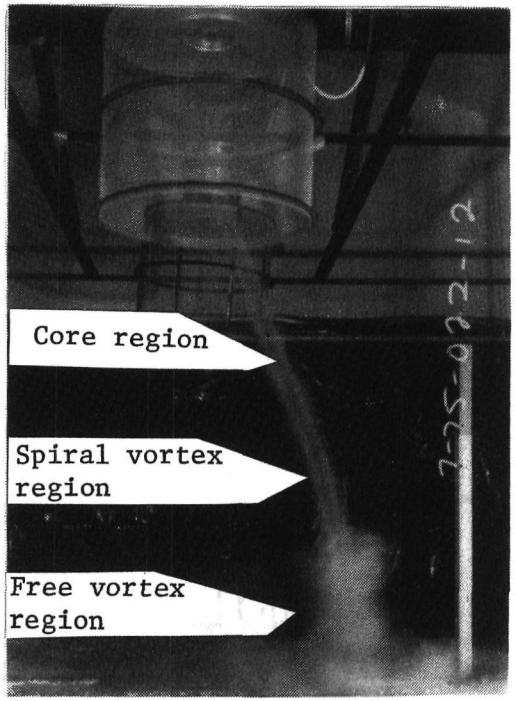

Figure 3.1.1 Single vortex - strong core flow

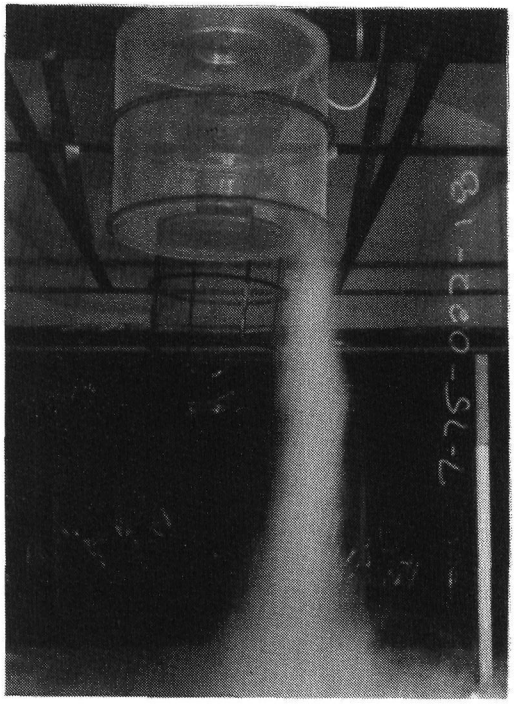

Figure 3.1.2 Single vortex - weakening core flow

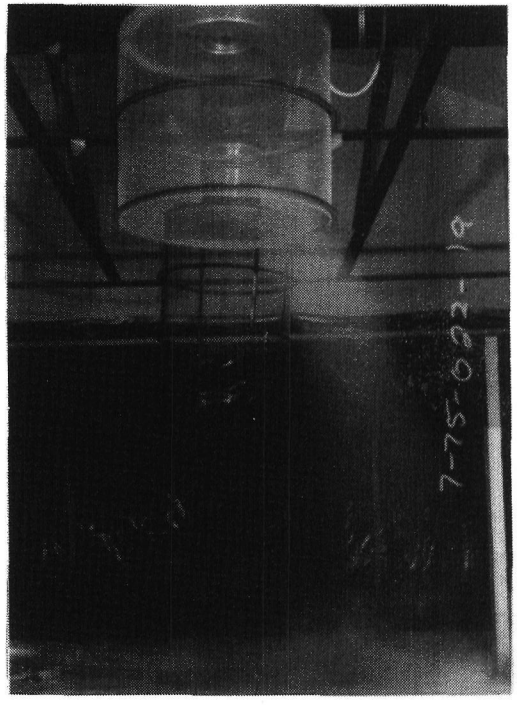

Figure 3.1.3 Single vortex - weakening core flow and cage interference

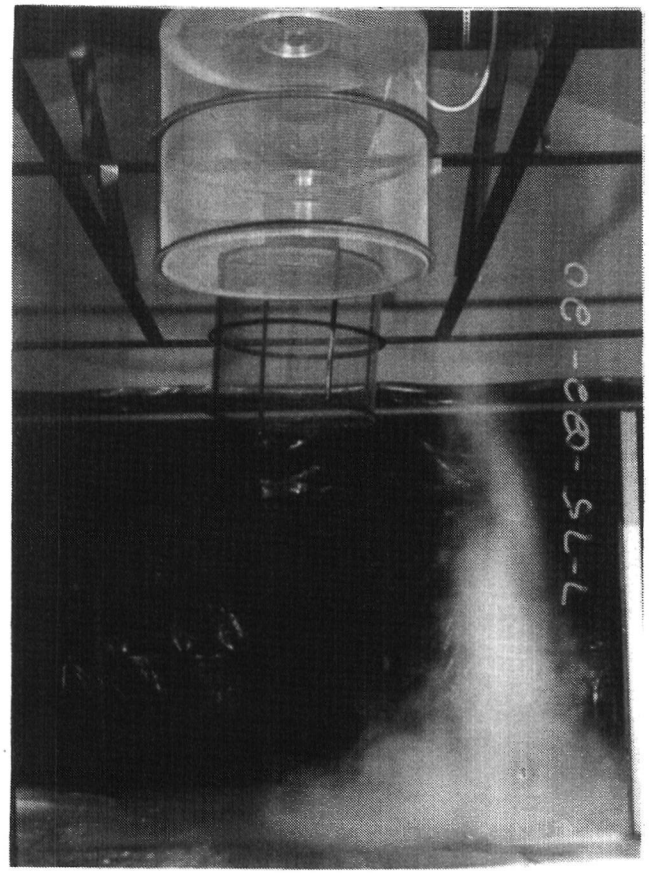

Figure 3.1.4 Single vortex - weakening detached core

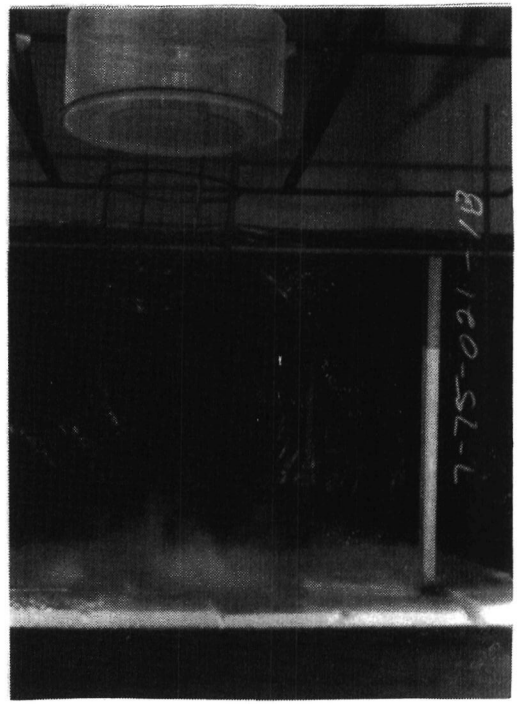

Figure 3.1.5 Single vortex - reforming

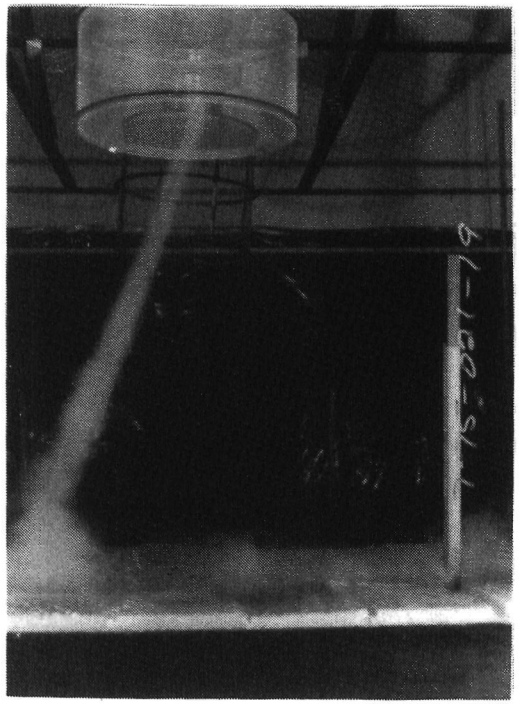

Figure 3.1.6 Single vortex - strong core flow with cross flow

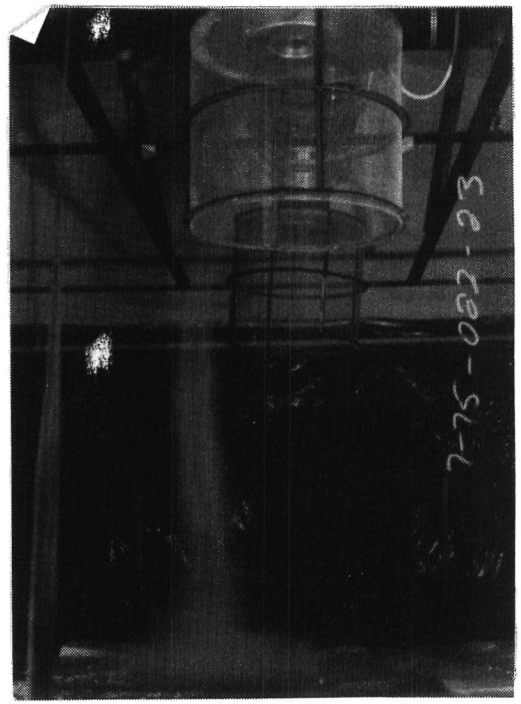

Figure 3.1.7 Single vortex - strong core flow - no rotation of cage

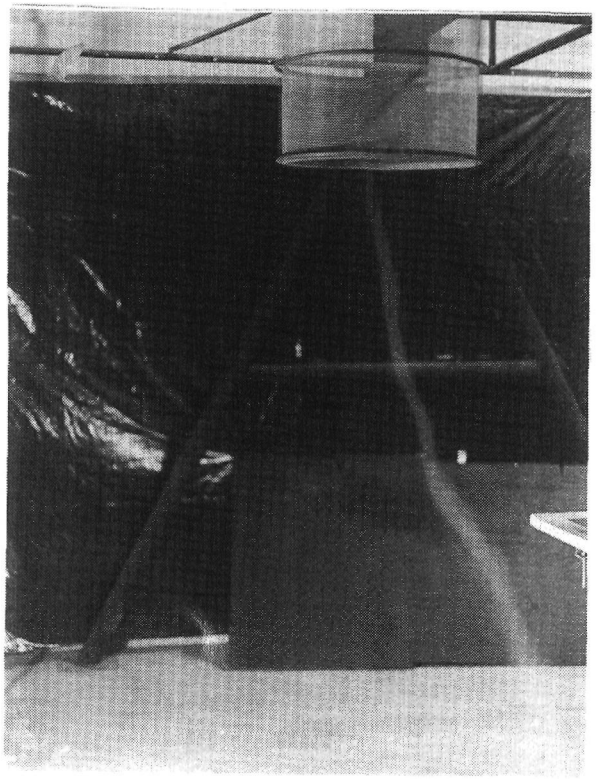

Figure 3.1.8 Single Vortex - 1200 r.p.m. steady cage rotation and axial pressure

Figure 3.2.1 Single vortex - initiation of vortex

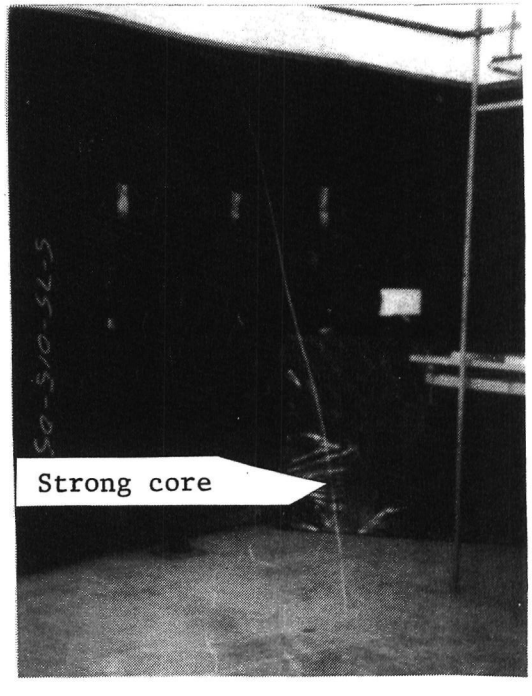

Figure 3.2.2 Single vortex - establishment of strong core flow

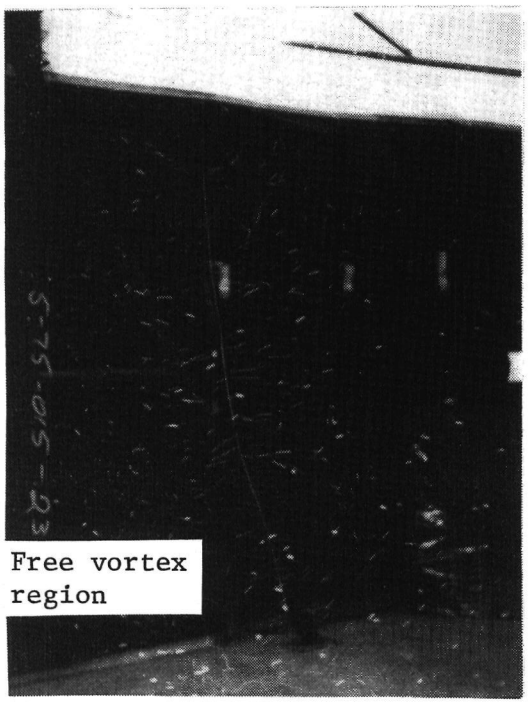

Figure 3.2.3 Single vortex - strong core flow

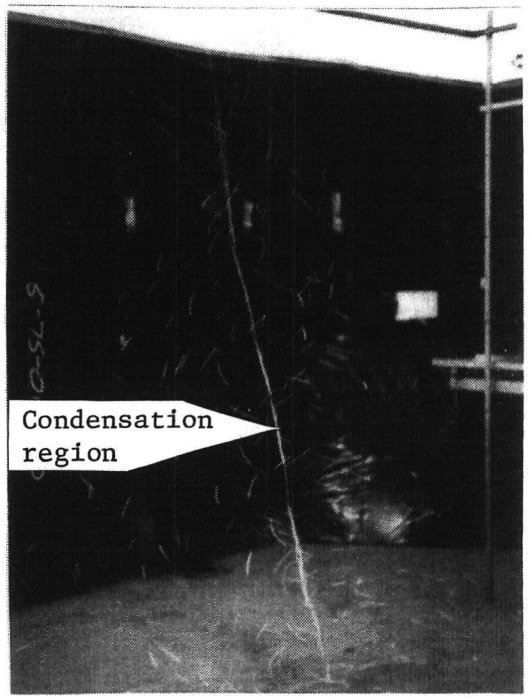

Figure 3.2.4 Single vortex - core flow slowing

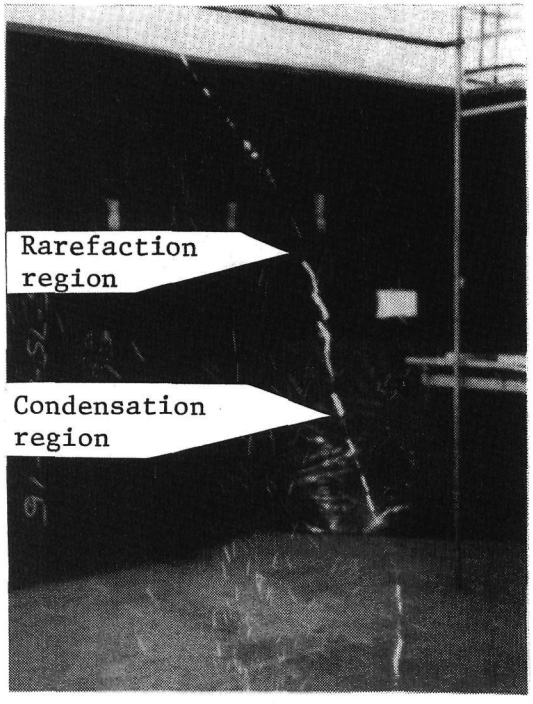

Figure 3.2.5 Single vortex - onset of core flow breakdown

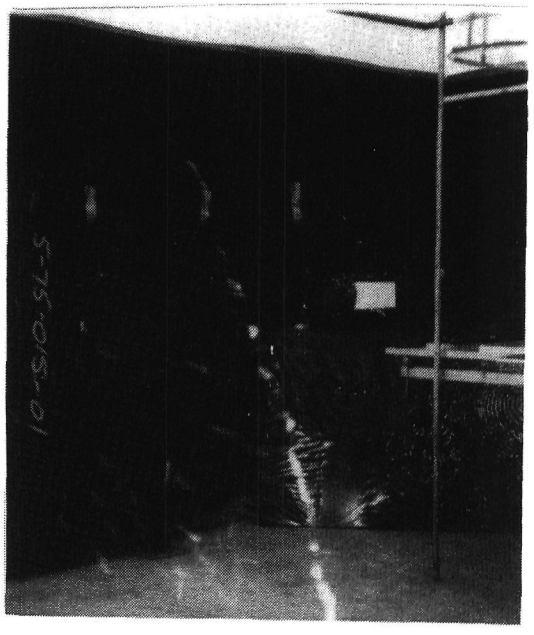

Figure 3.2.6 Single vortex - core flow breakdown

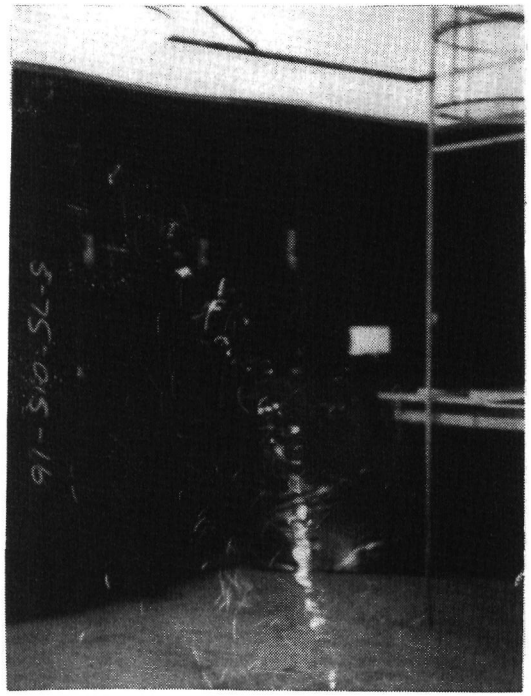

Figure 3.2.7 Single vortex - breakdown

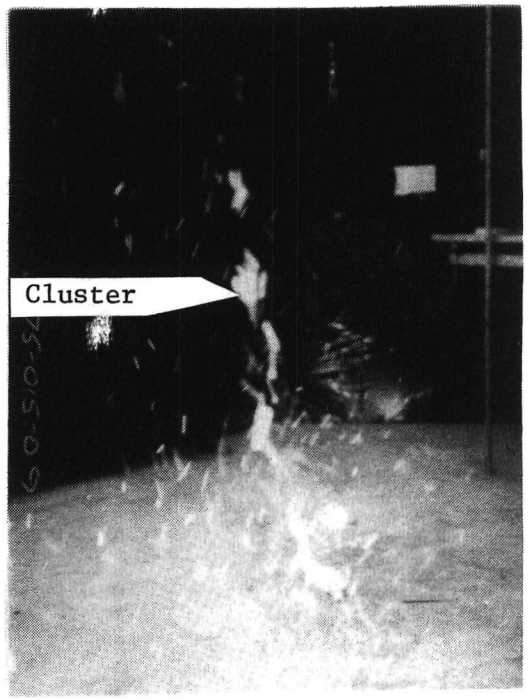

Figure 3.2.8 Single vortex - breakdown, final stages

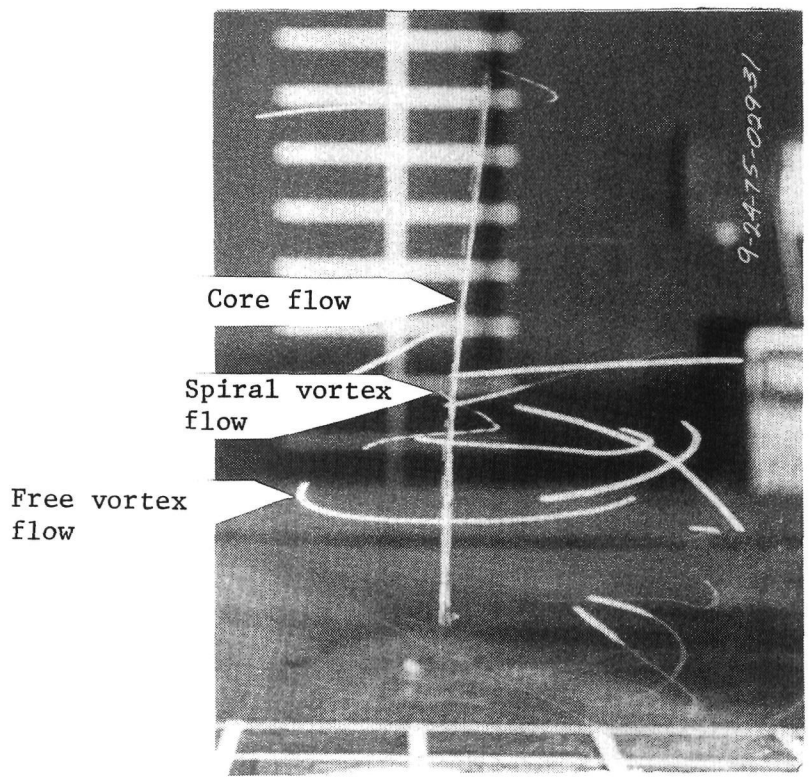

Figure 3.3.1 Single vortex core, spiral and free vortex flows

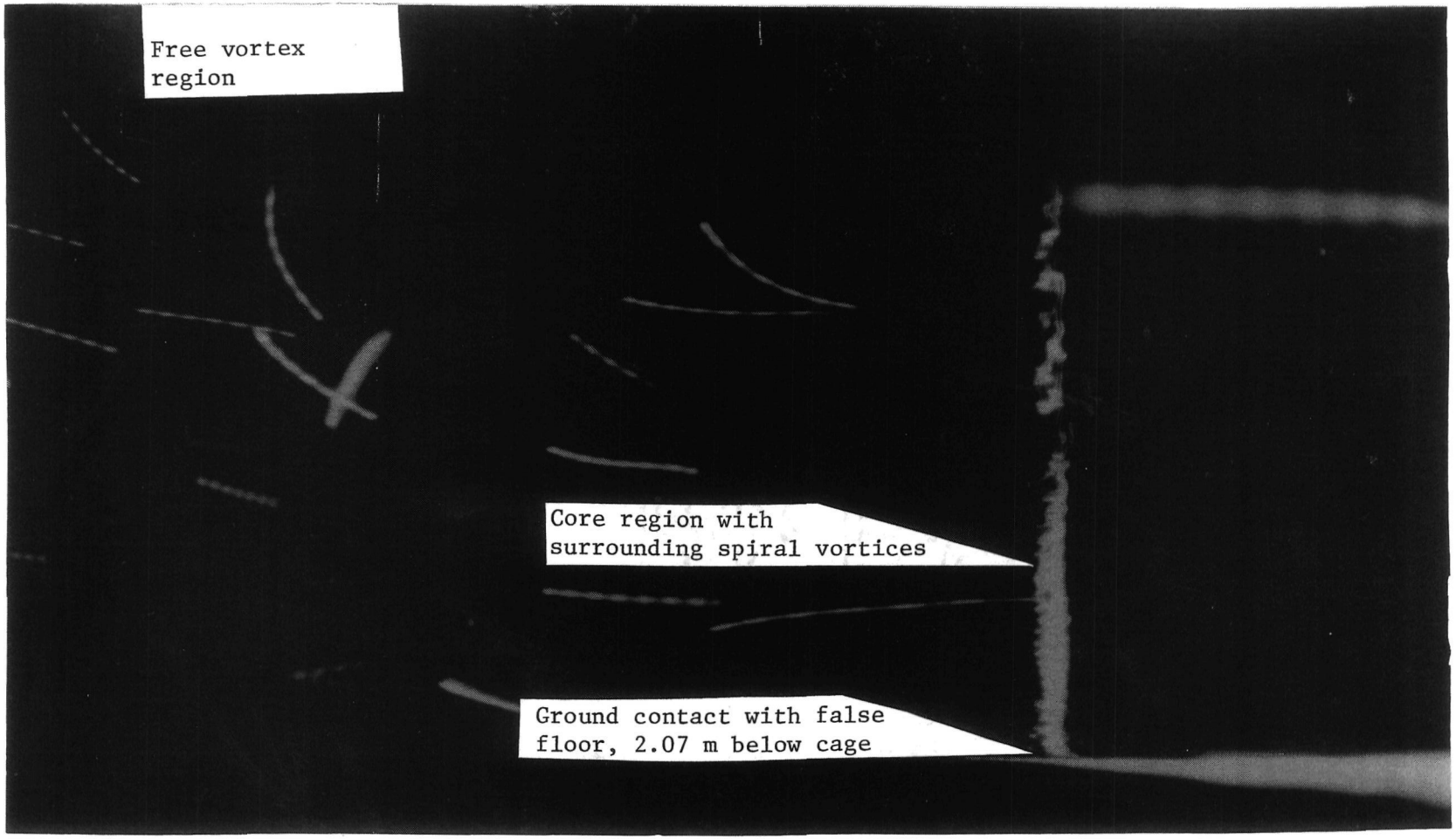

Figure 3.3.2 Core flow at ground contact

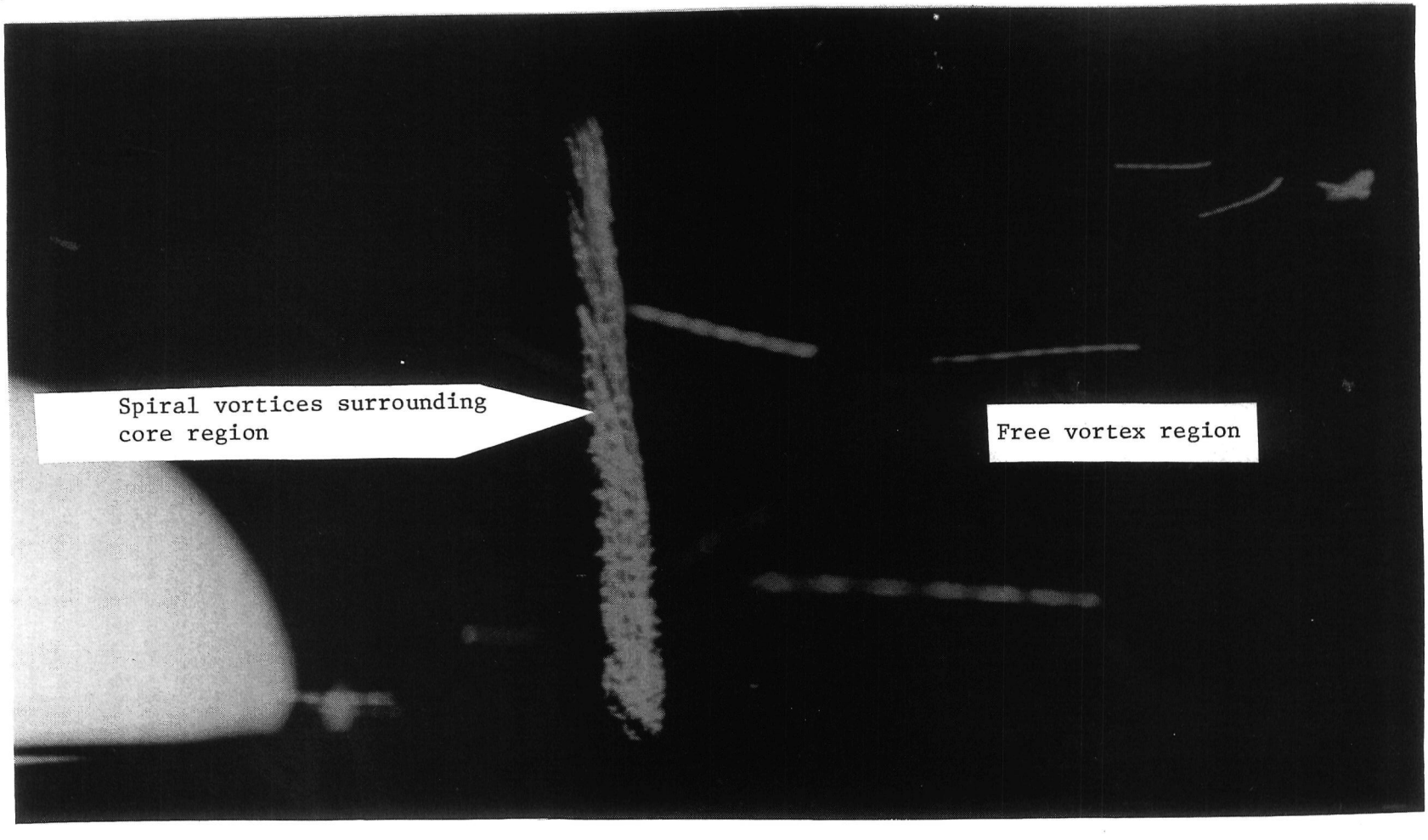

Figure 3.3.3 Core flow increasing - near ground

Figure 3.3.4 Core flow increasing - particle flows near ground

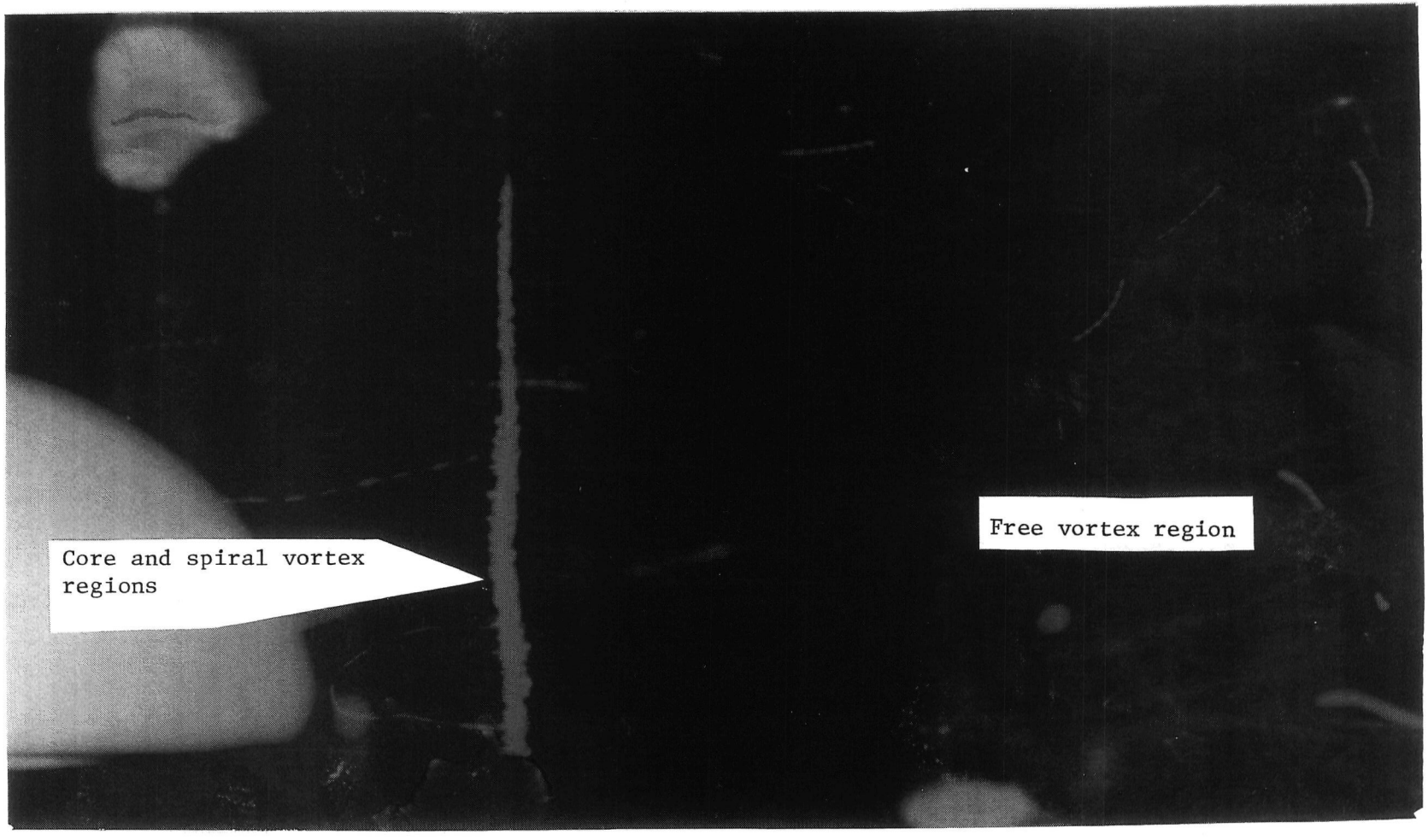

Figure 3.3.5 Strong core flow - near ground

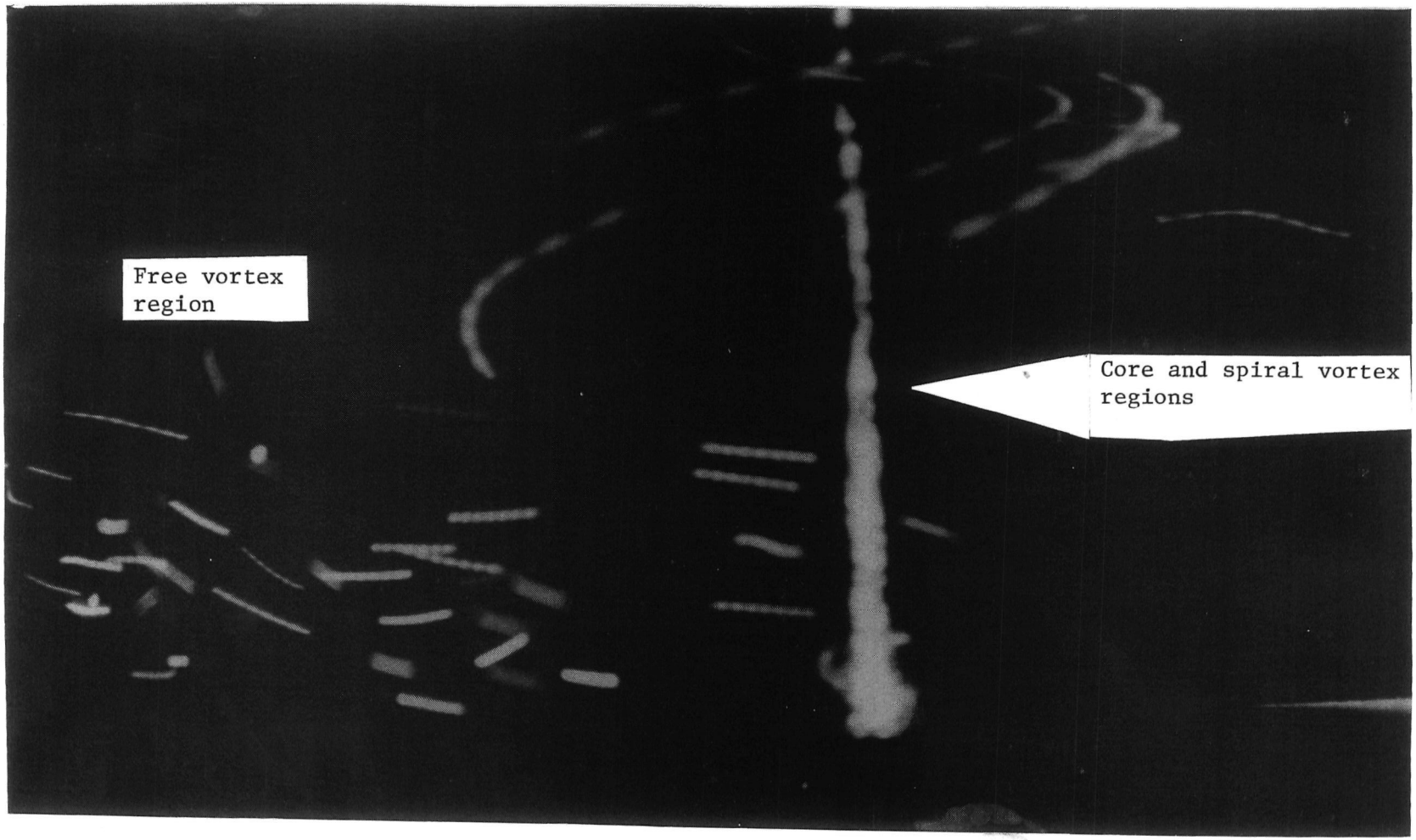

Figure 3.3.6 Core flow decreasing - near ground

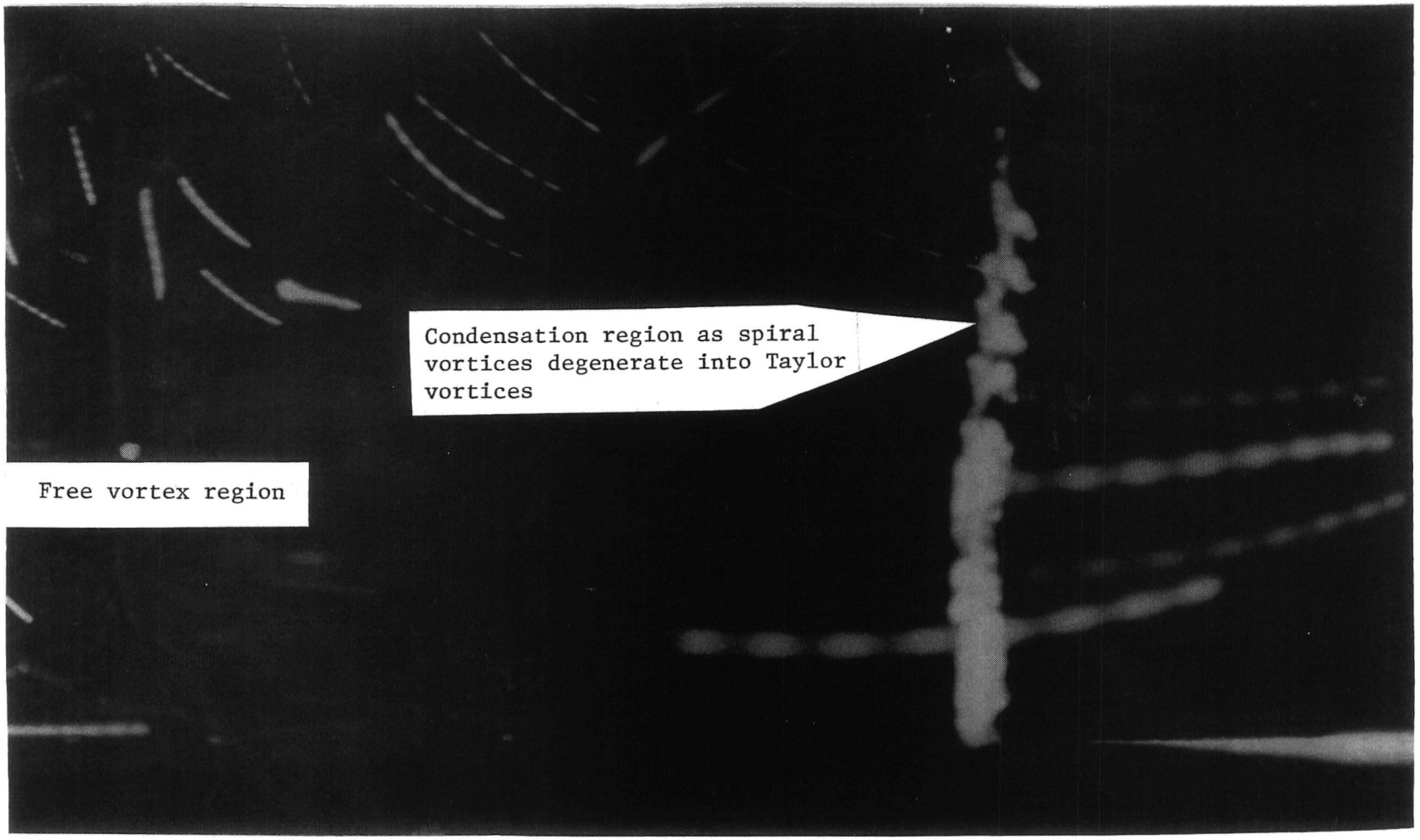

Figure 3.3.7 Core flow - onset of core flow breakdown near ground

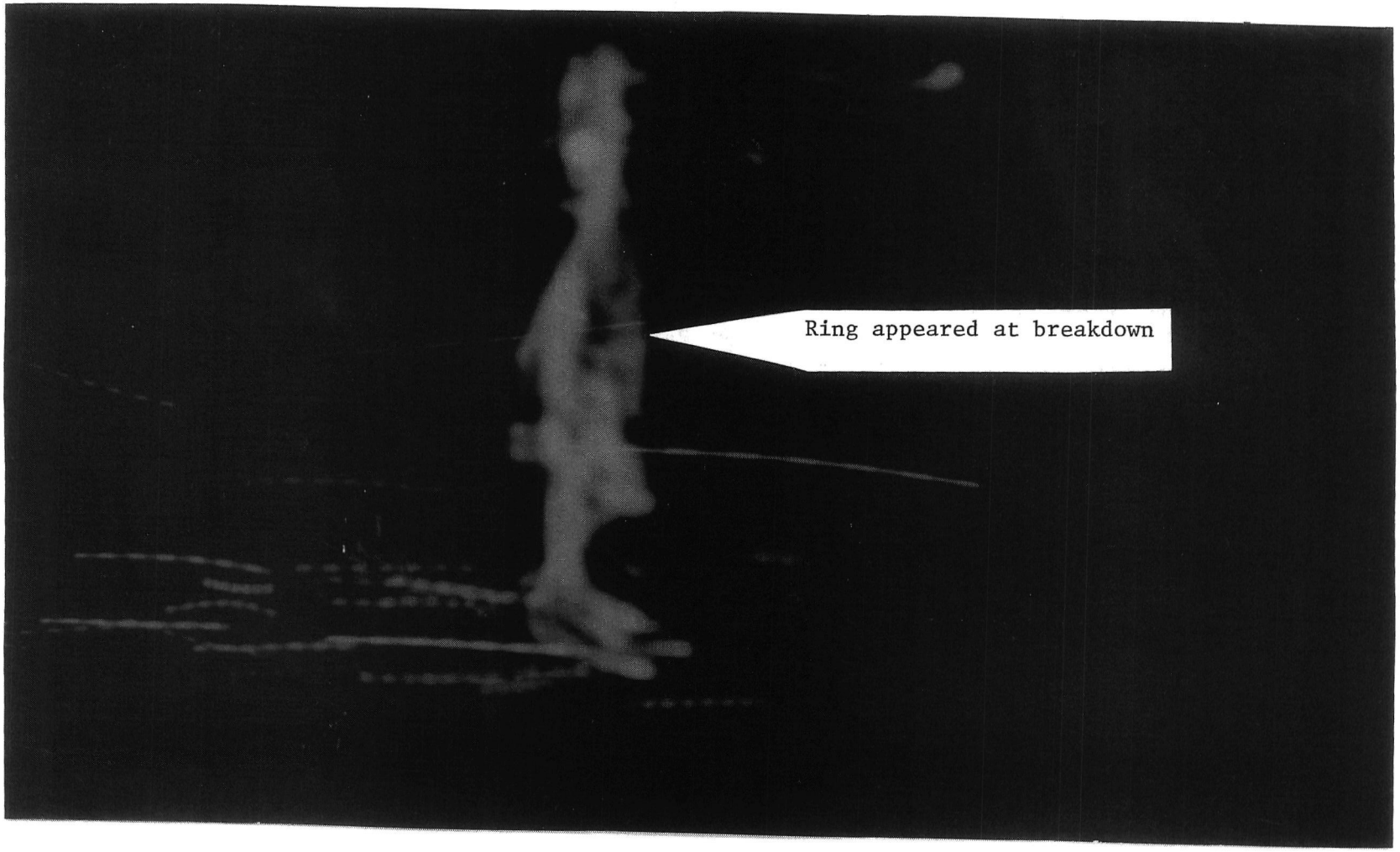

Figure 3.3.8 Core flow breakdown - near ground

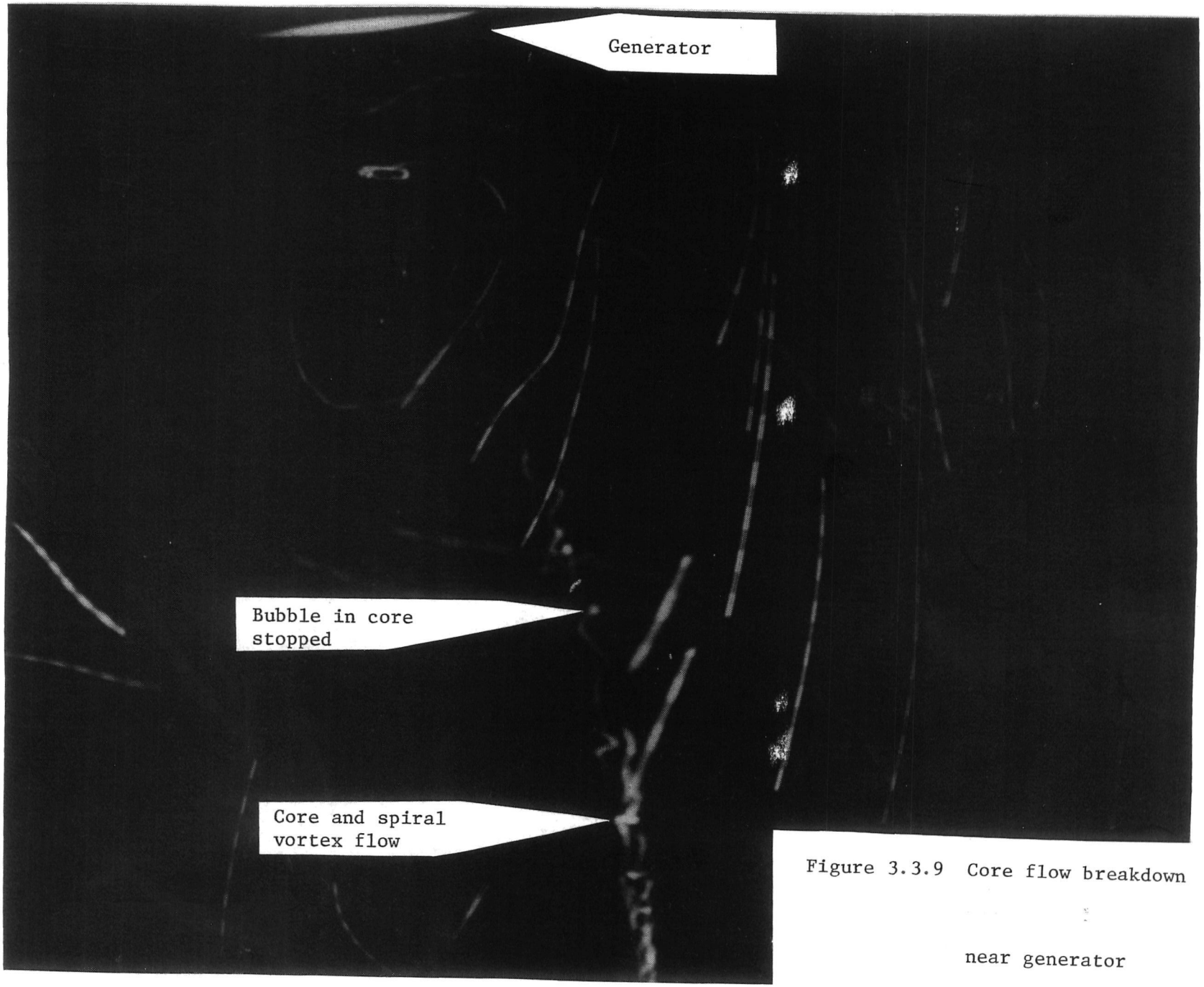

Figure 3.3.9 Core flow breakdown near generator

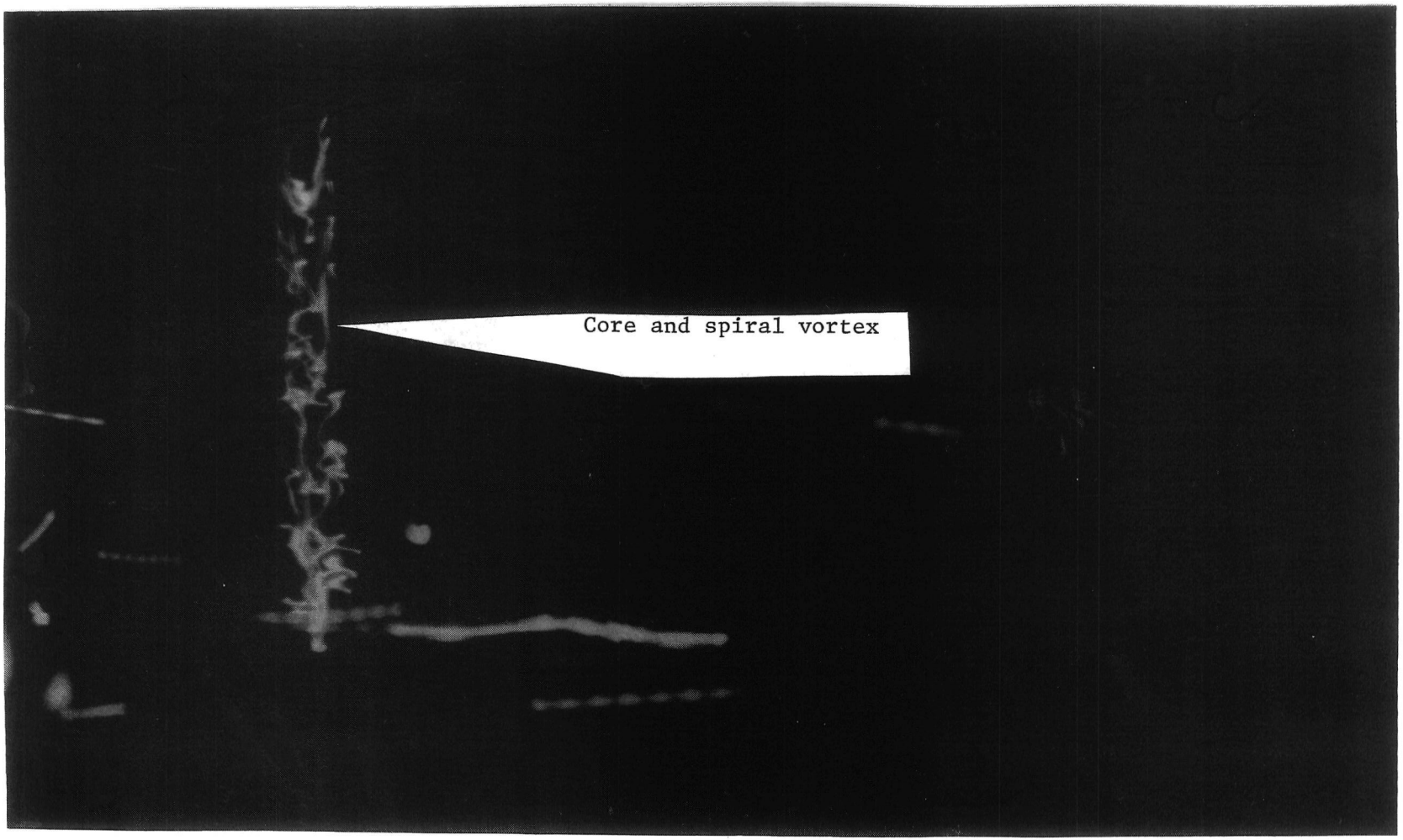

Figure 3.3.10 Core flow breakdown - near ground

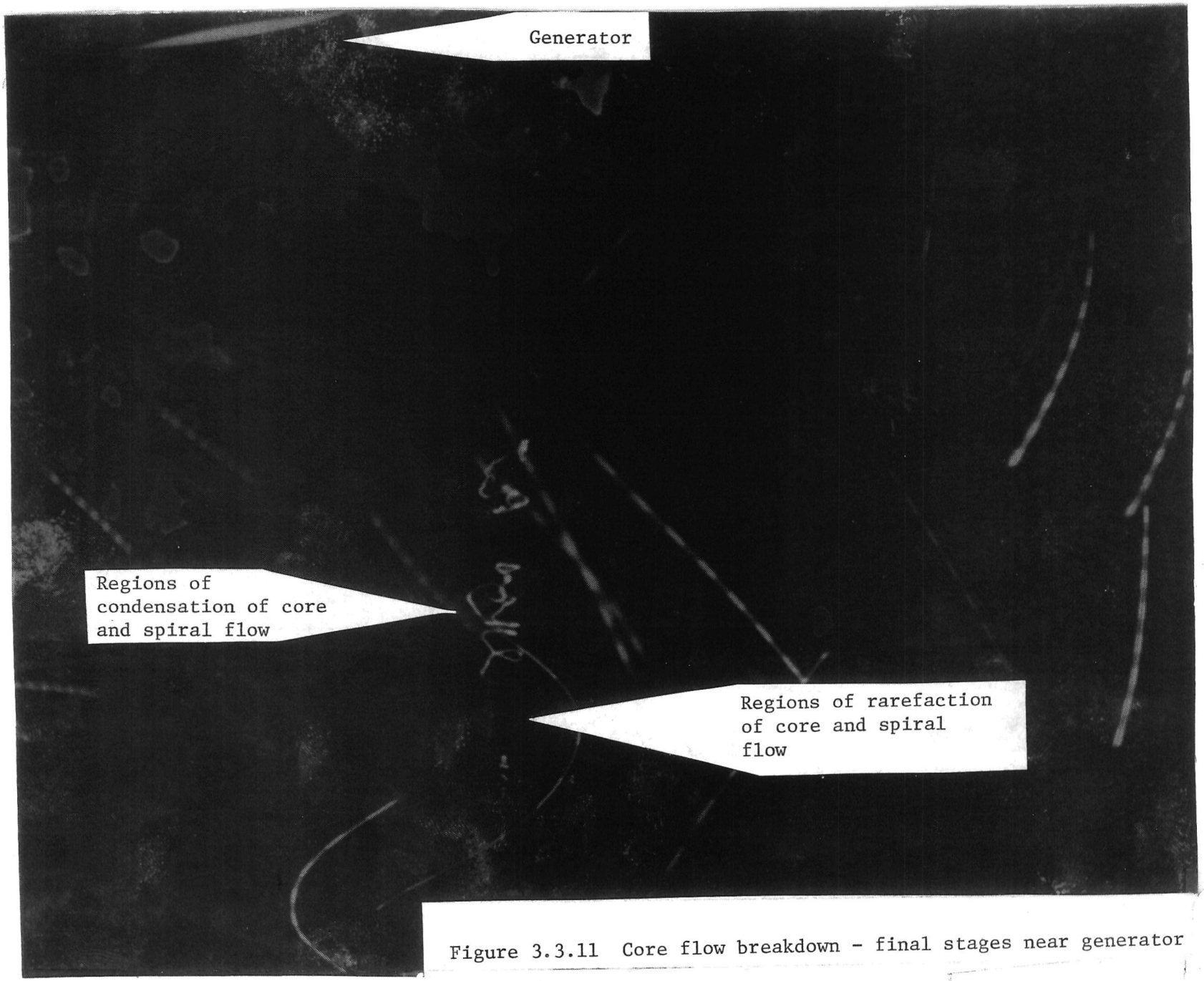

Figure 3.3.11 Core flow breakdown - final stages near generator

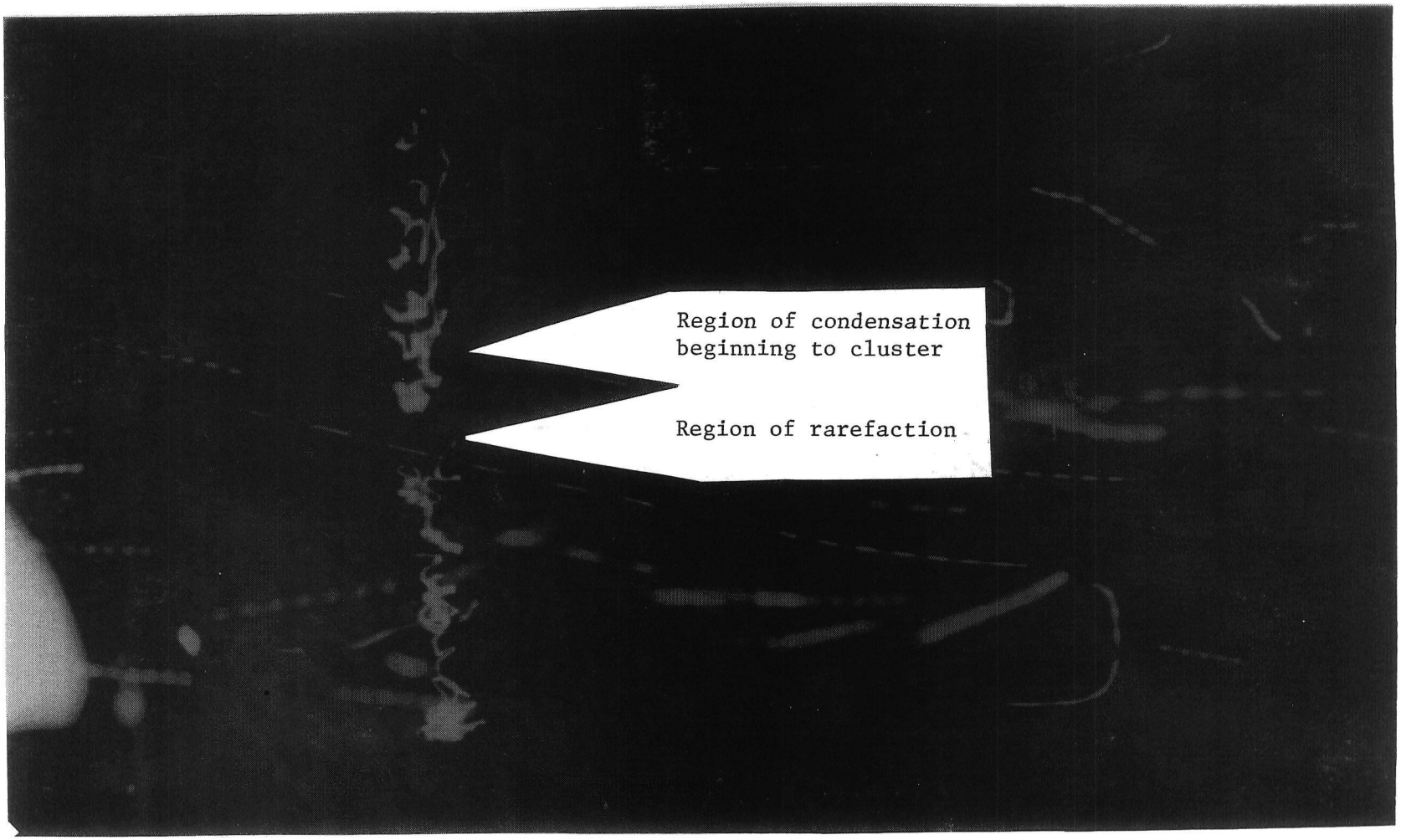

Figure 3.3.12 Core flow breakdown - final stages near ground

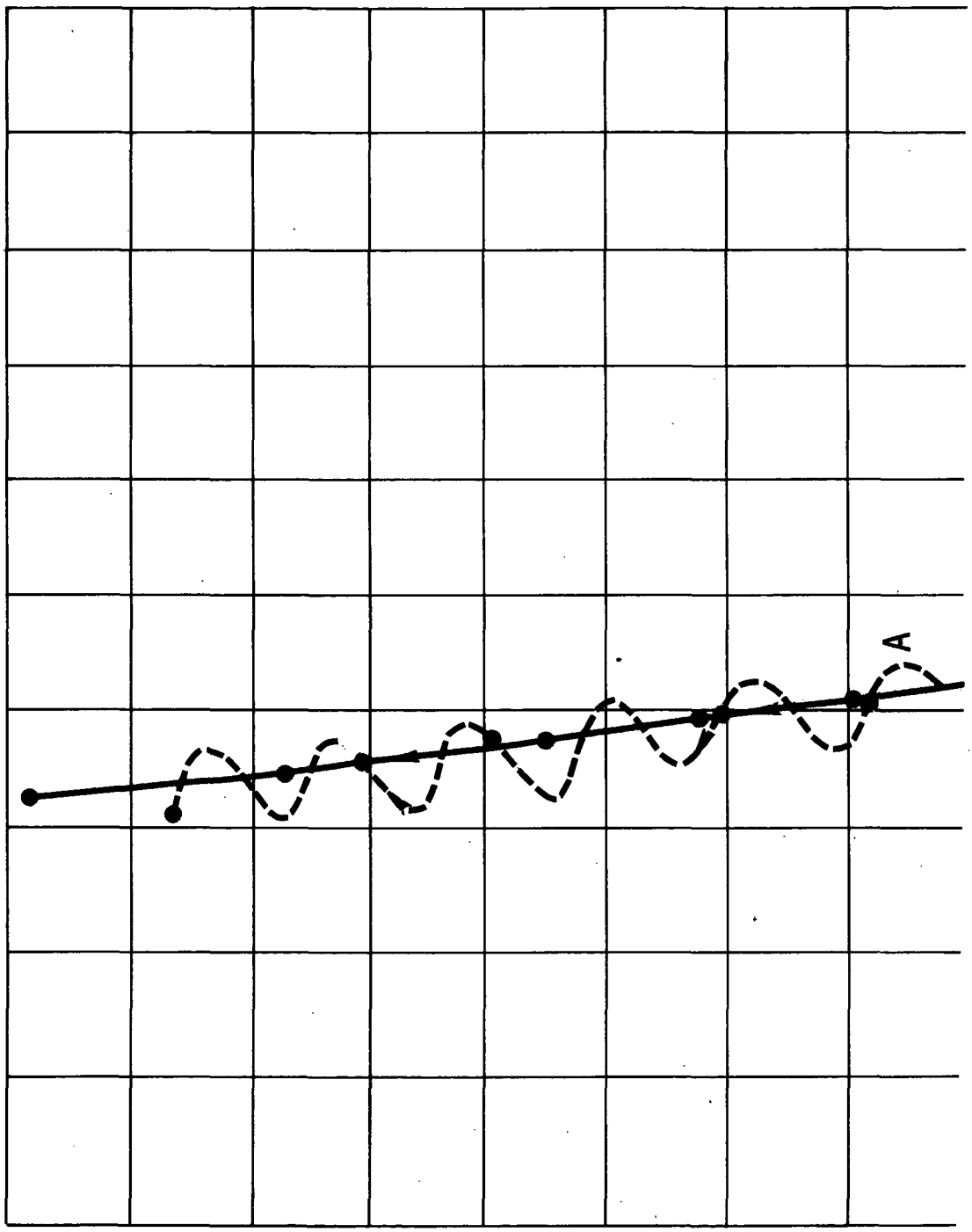

Figure 3.4.1 Bubble paths - strong core flow

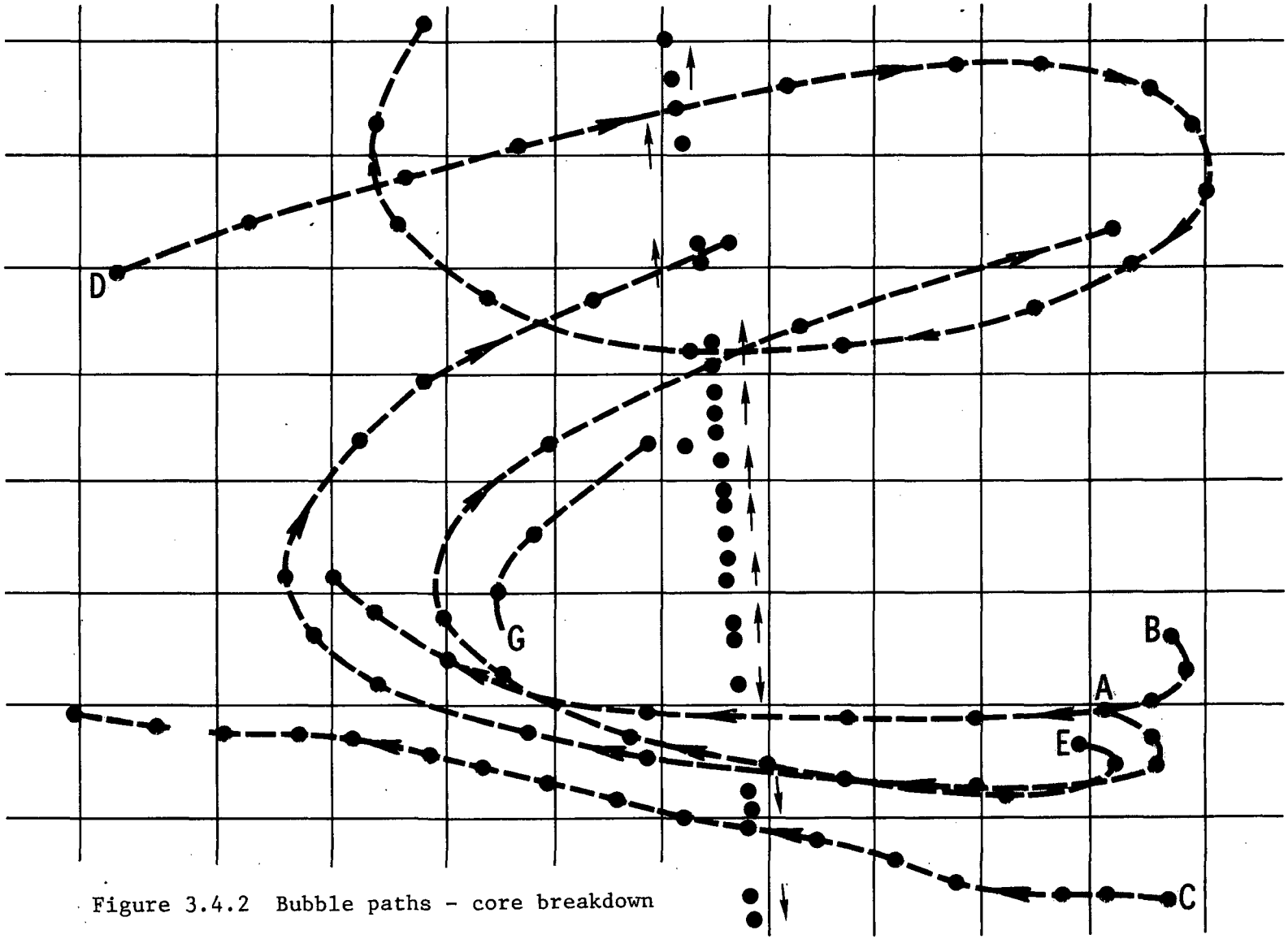

Figure 3.4.2 Bubble paths - core breakdown

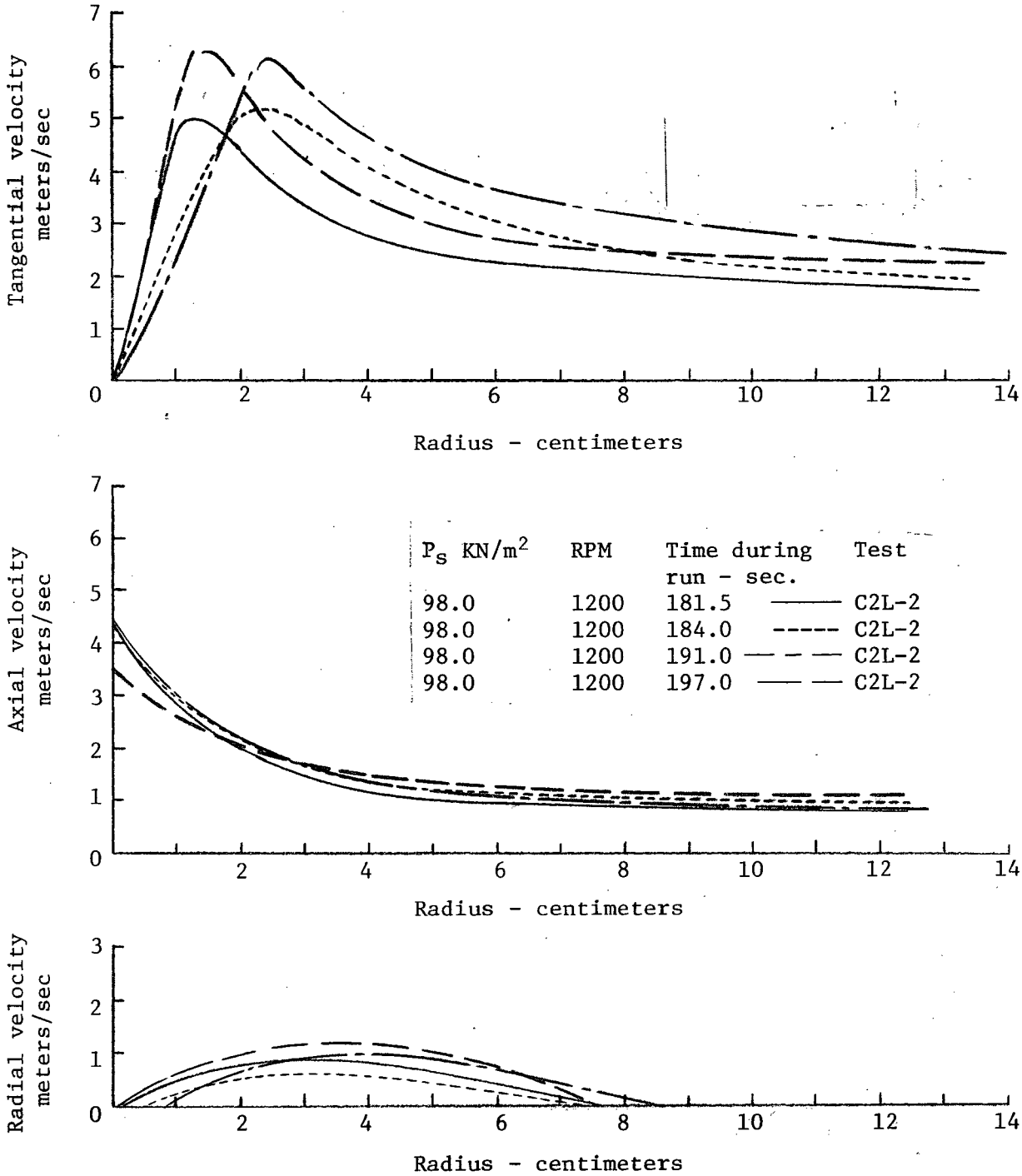

Figure 3.4.3 Velocity components at low position with small nozzle, steady cage rotation and no externally applied pressure at nozzle

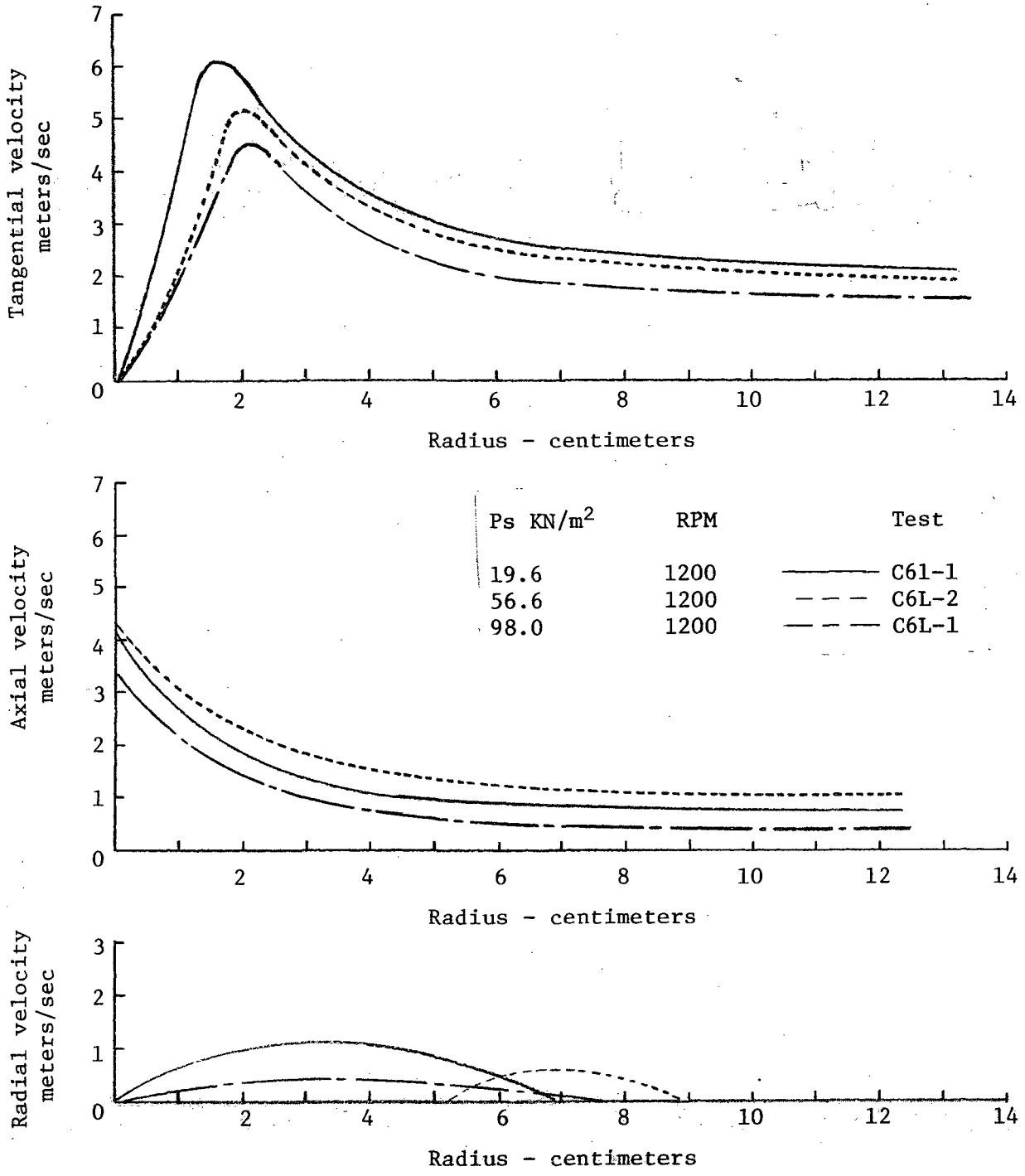

Figure 3.4.4 Velocity components at low position with medium nozzle, steady cage rotation and applied pressure decay

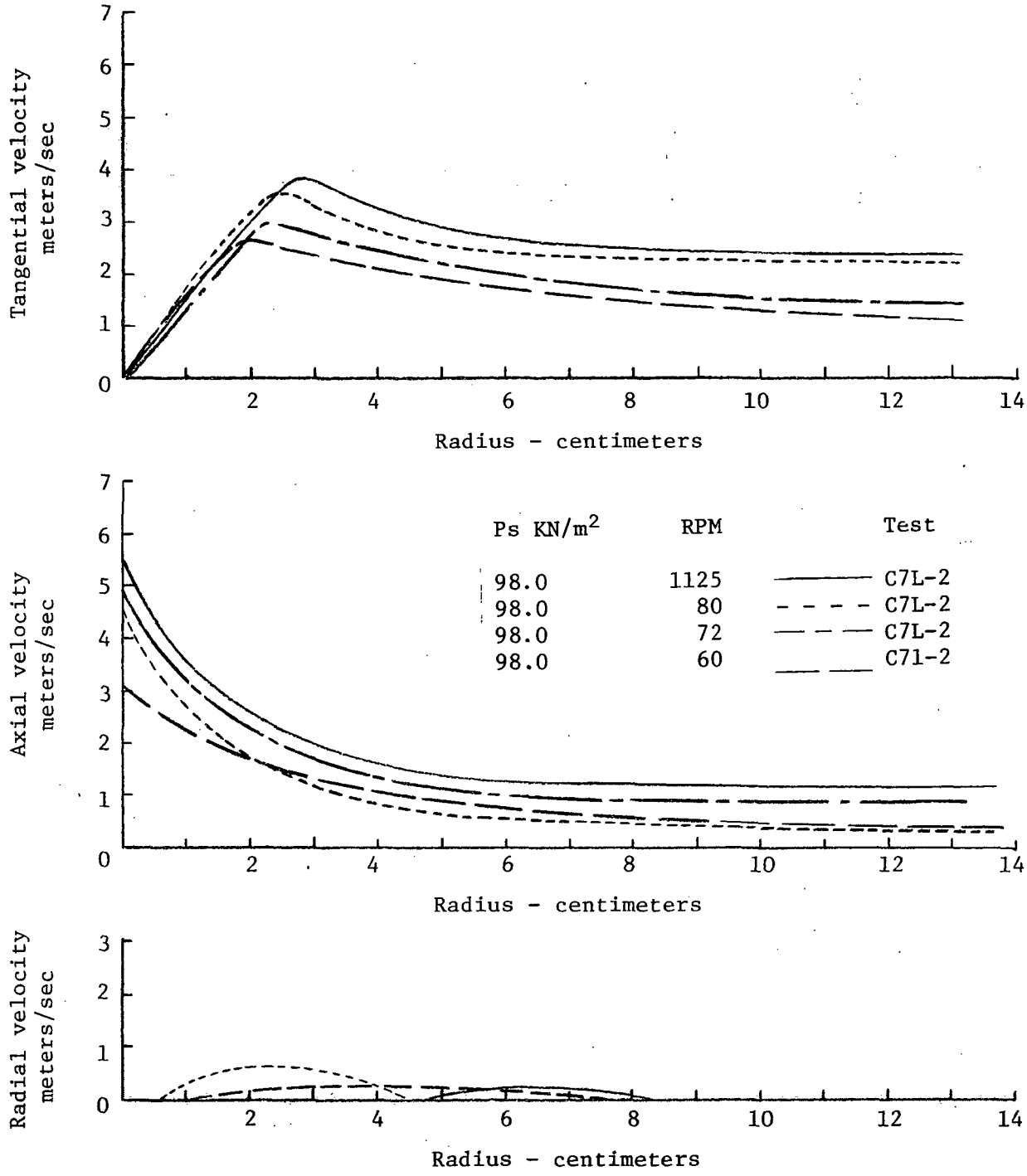

Figure 3.4.5 Velocity at low position with medium nozzle, decaying cage rotation and no externally applied pressure

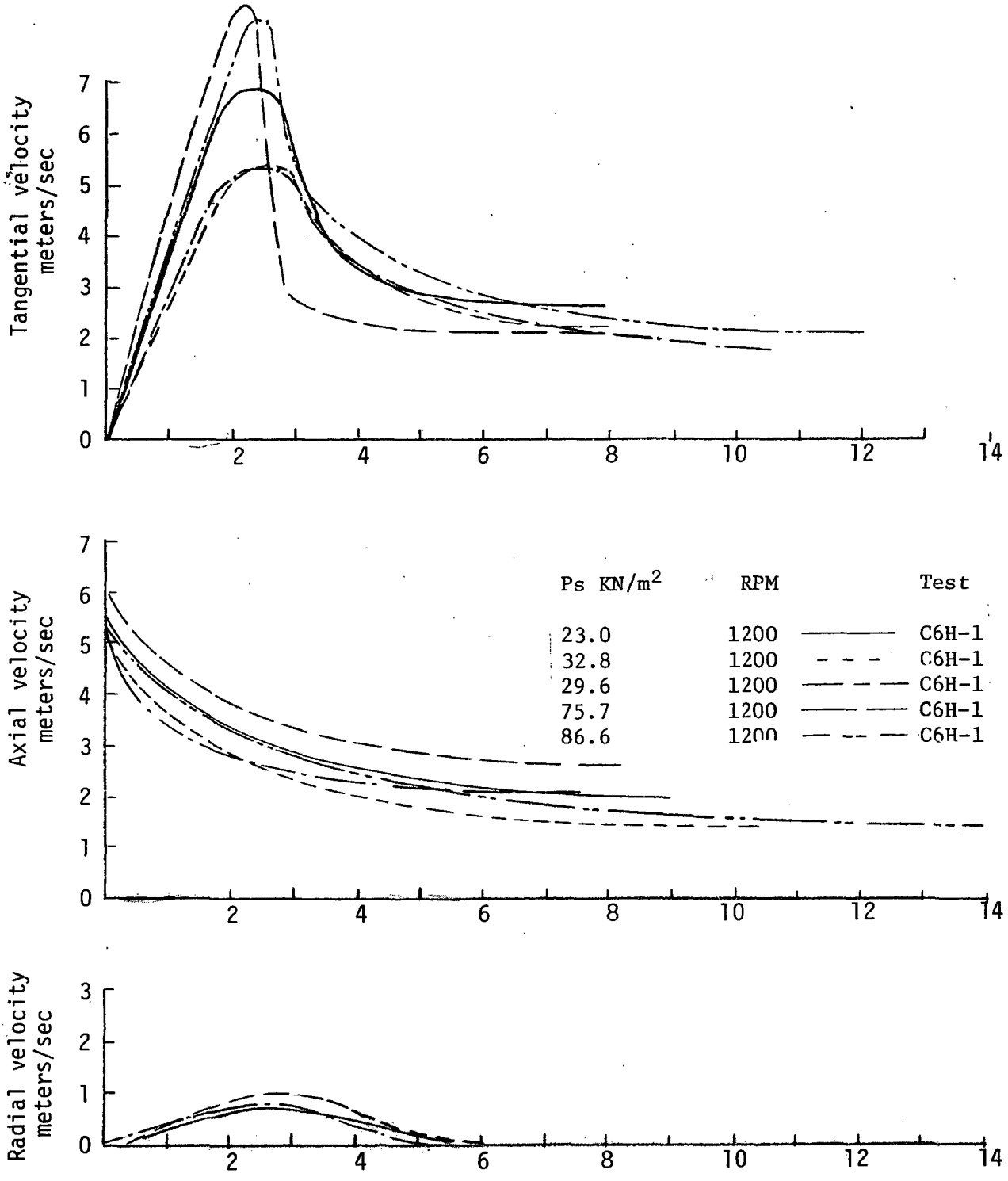

Figure 3.4.6 Velocity components at high position with medium nozzle, steady cage rotation and pressure decay

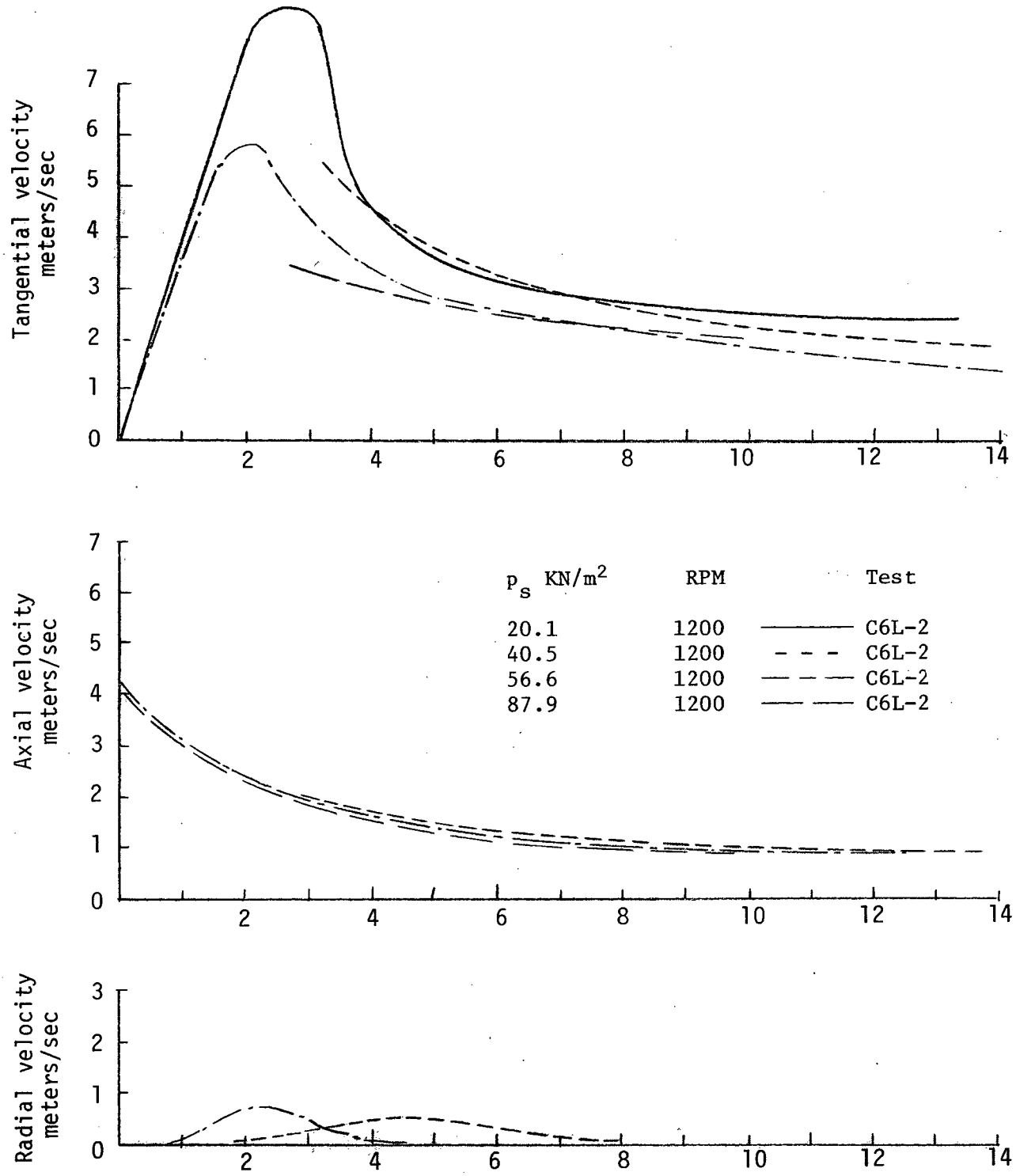

Figure 3.4.7 Velocity components at low position with medium nozzle, steady cage rotation and pressure decay

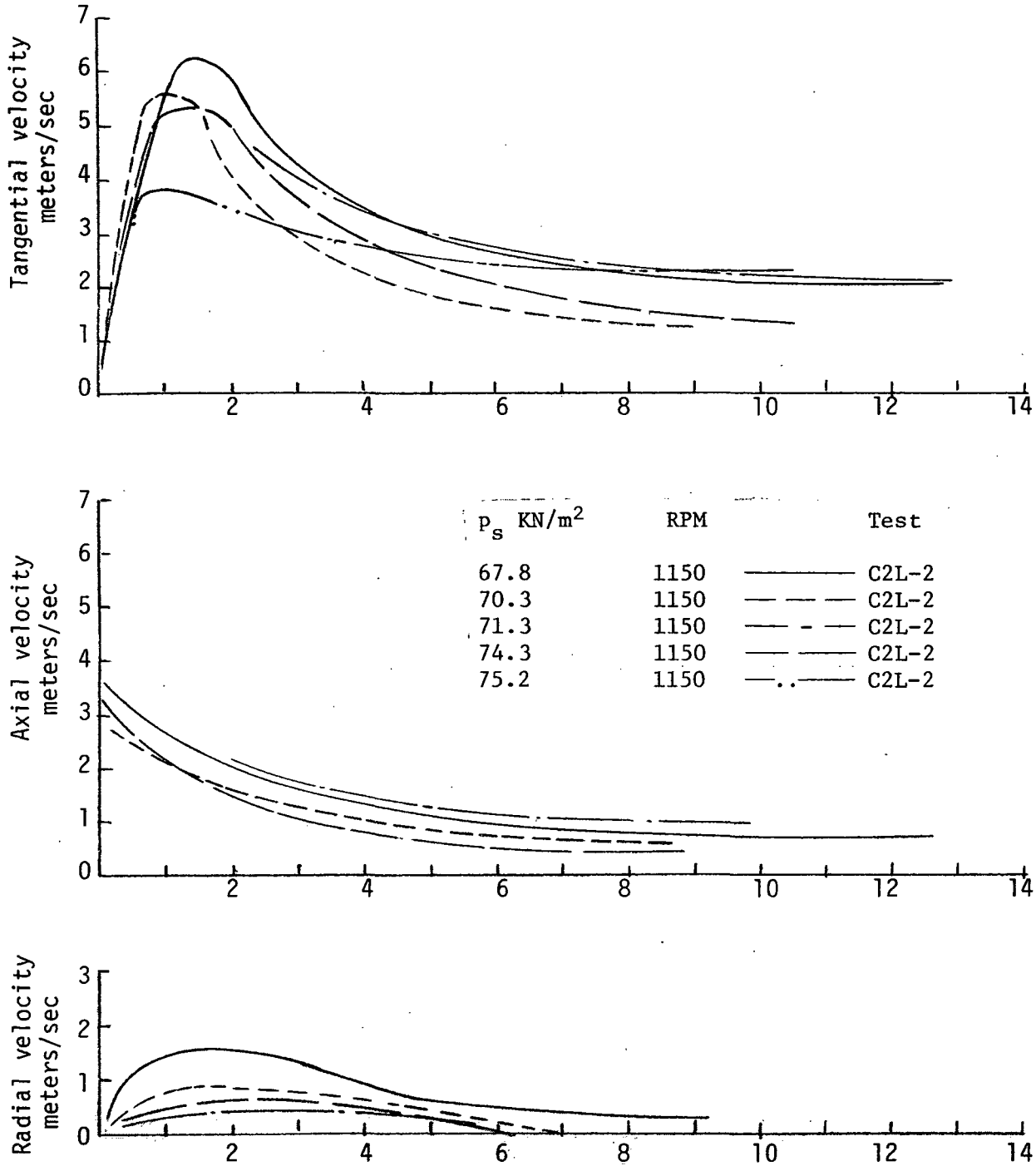

Figure 3.4.8 Velocity components at low position with small nozzle, steady cage rotation and pressure decay

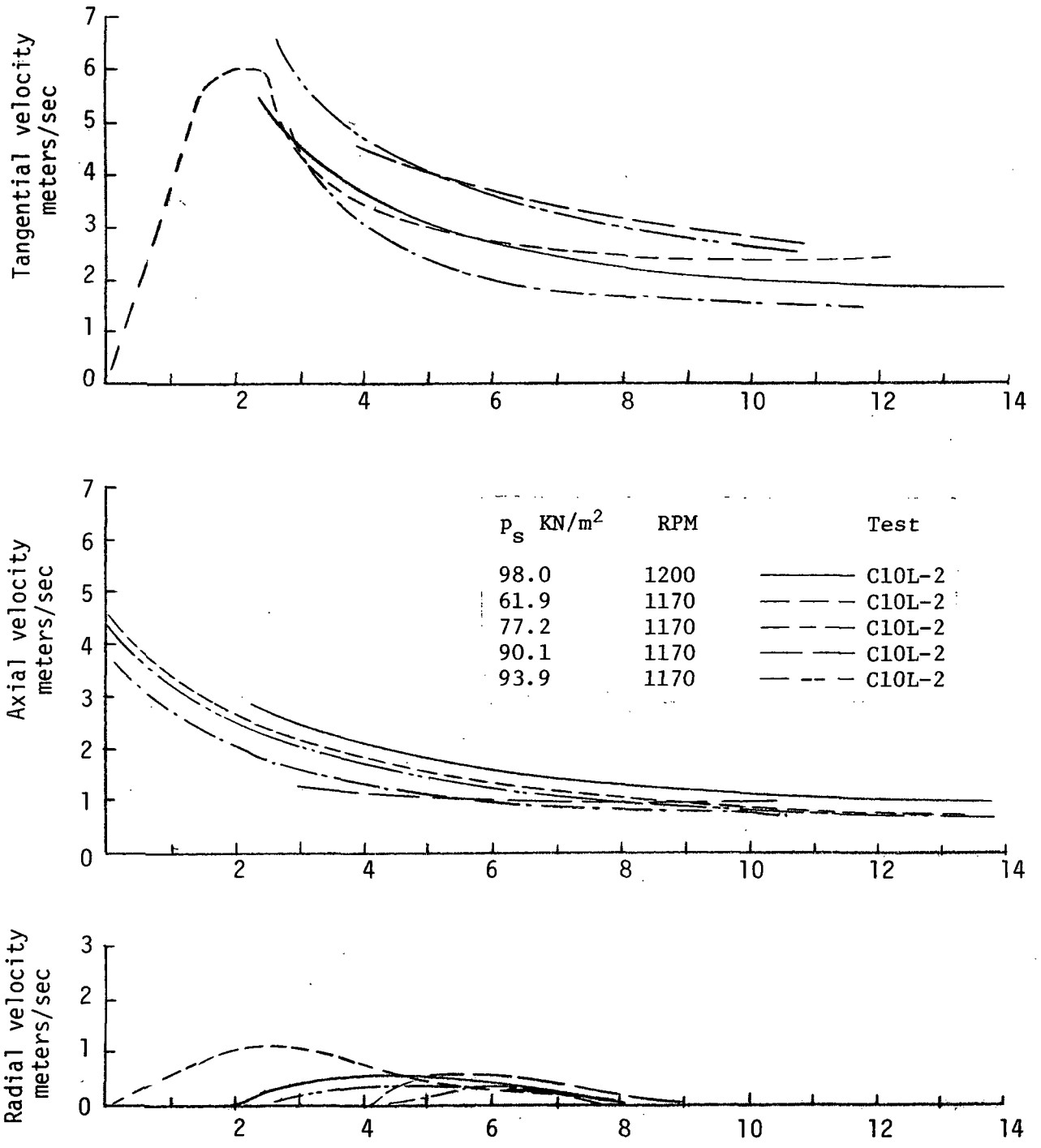

Figure 3.4.9 Velocity components at low position with large nozzle, steady cage rotation and pressure decay

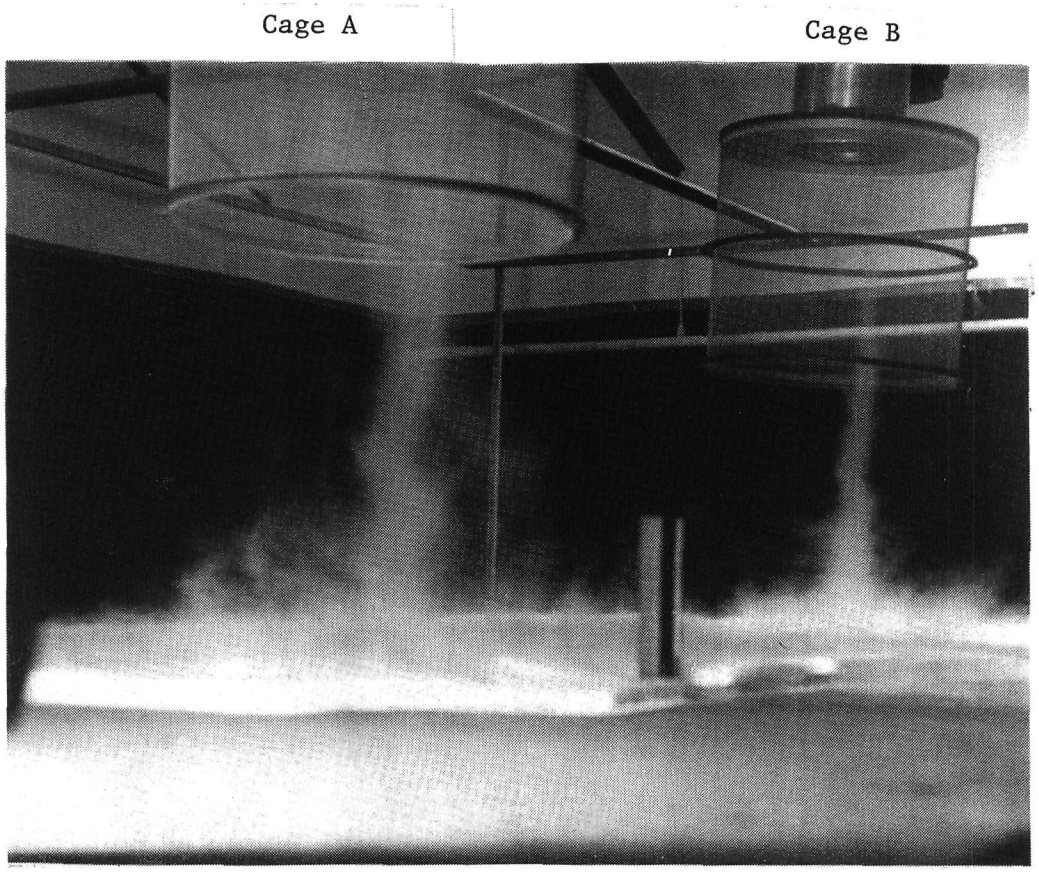

Figure 4.1.1 Dual vortices - spiral and core regions with increasing intensity - counter rotation

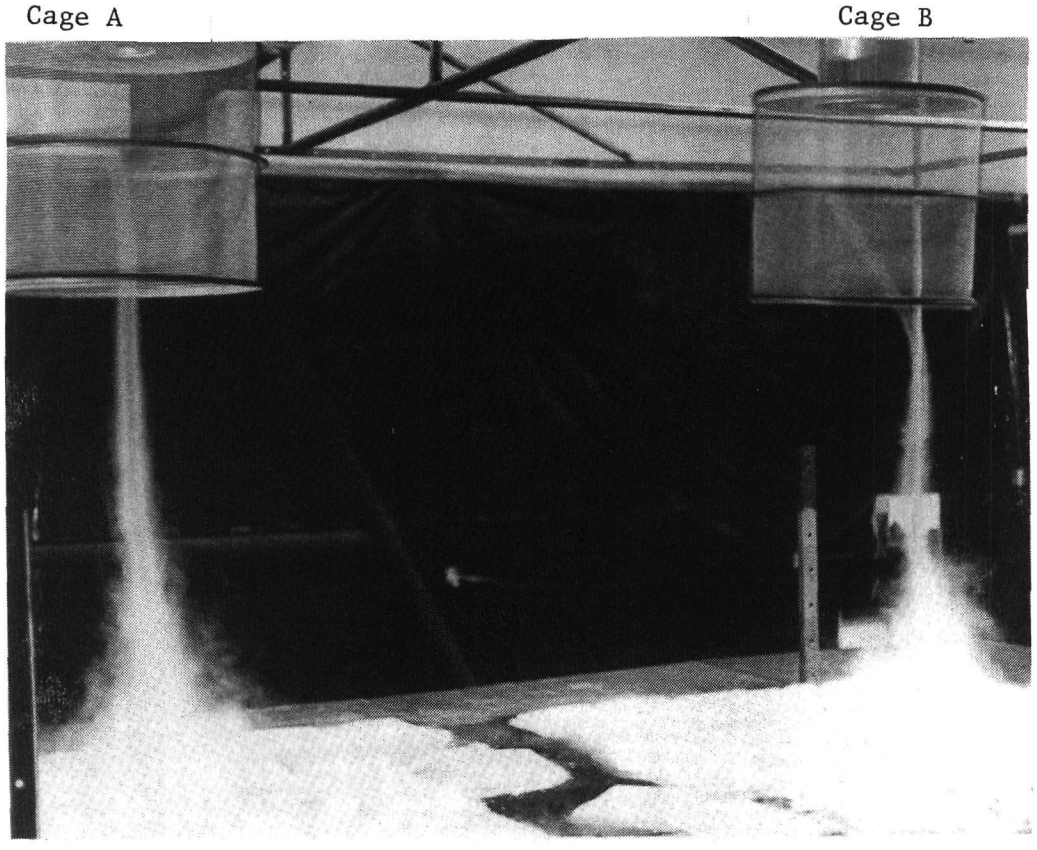

Figure 4.1.2 Dual vortices - maximum intensity - counter rotation

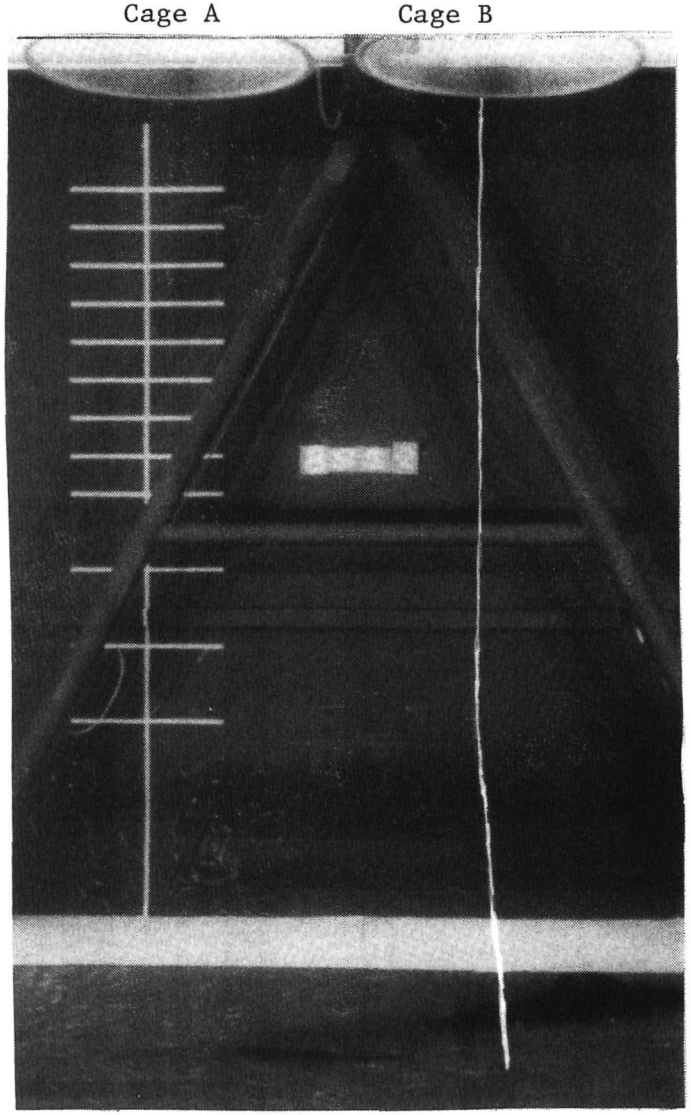

Figure 4.1.3 Corotating cages with single core

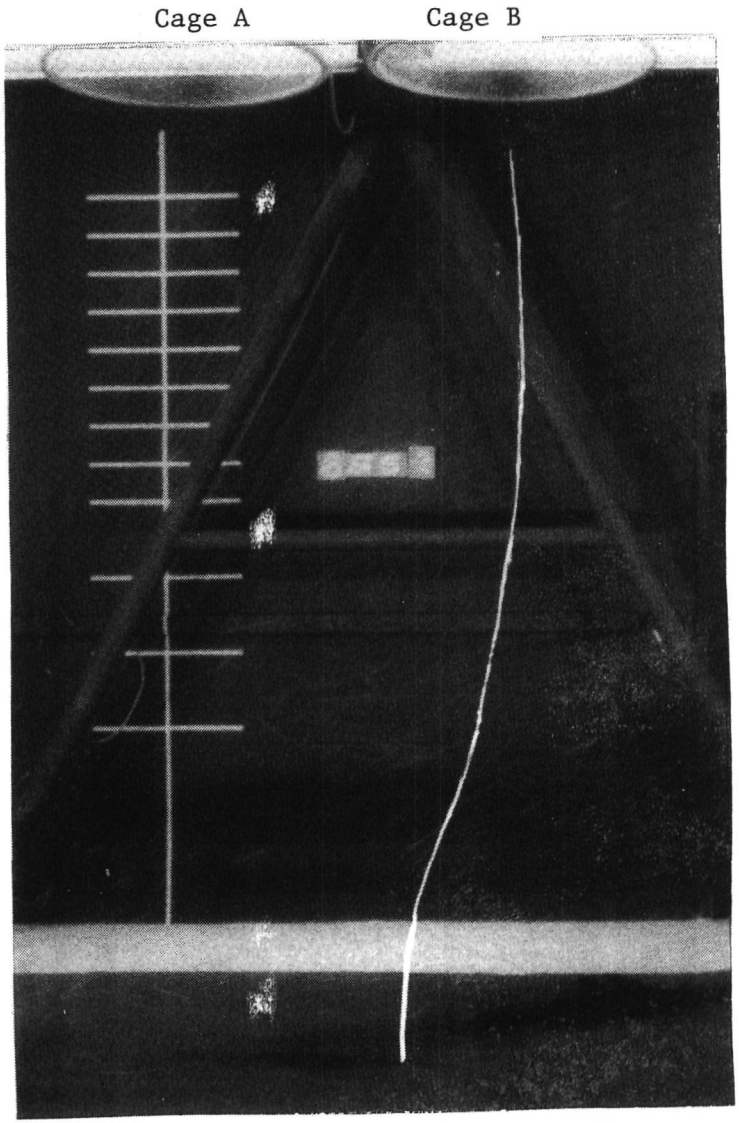

Figure 4.1.4 Corotating cages - core meandering

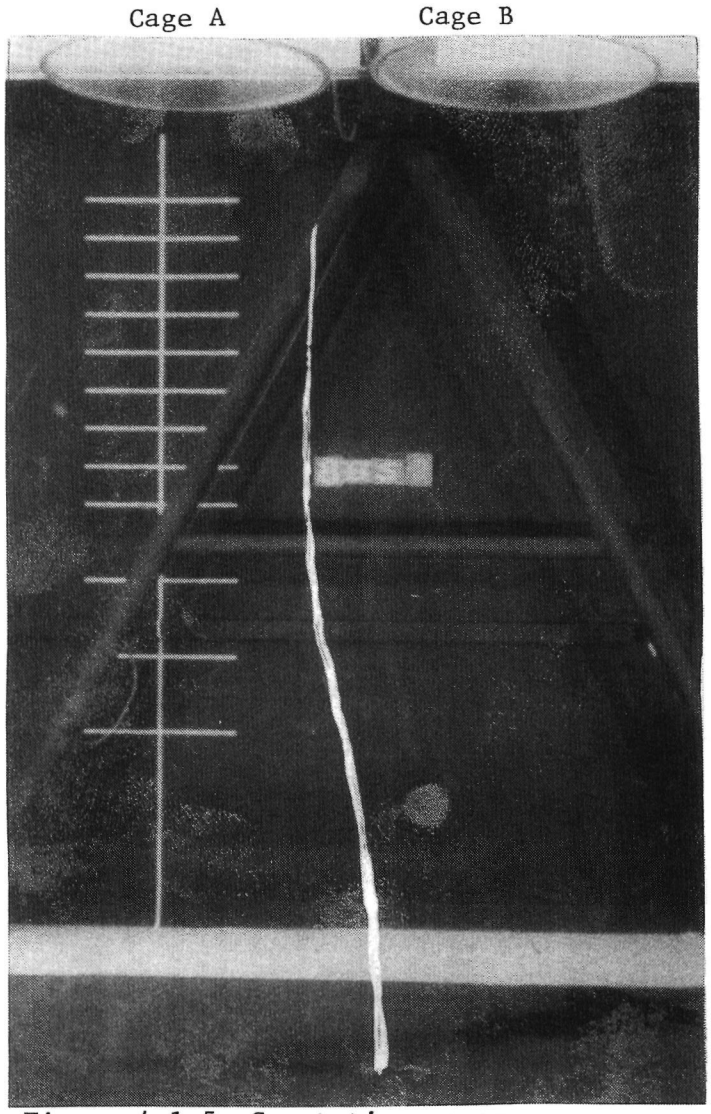

Figure 4.1.5 Corotating cages - weak core between cages

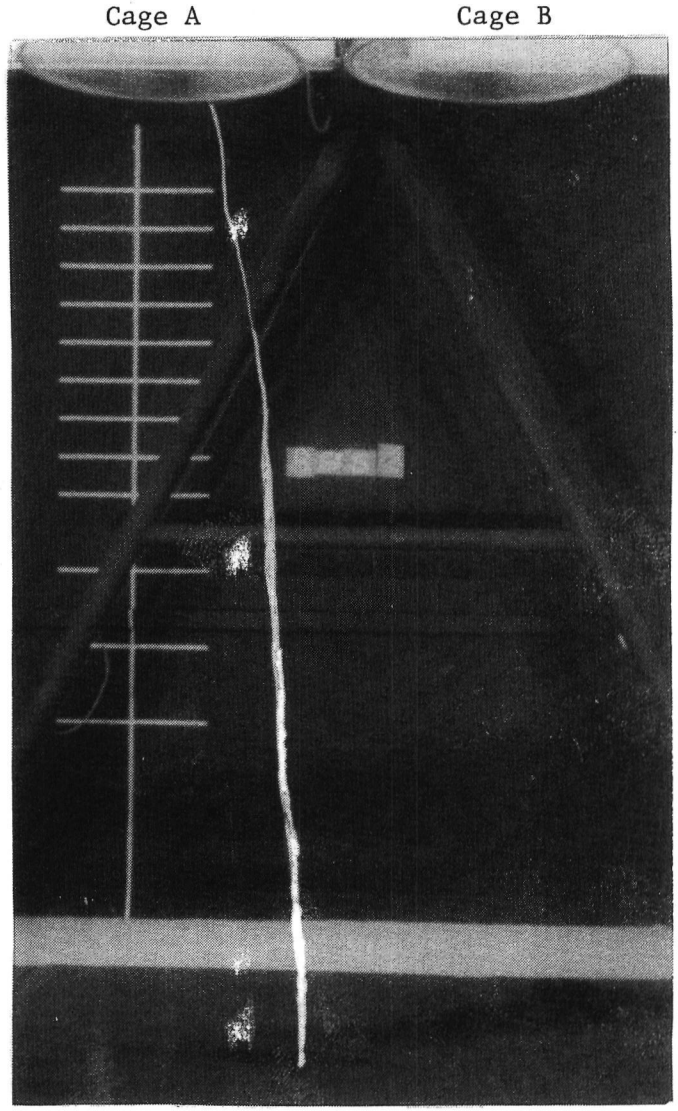

Figure 4.1.6 Corotating cages - core attached to second cage sink and strengthening

TABLE I

Single Vortex Test Parameters

Test No.	Camera Position	Nozzle Size	Pressure Decay	RPM (Initial)	RPM Decay
A1	Low	Small	No	600	No
A2	"	"	Yes	"	"
A3	"	"	"	"	Yes
A4	"	"	" (5 sec delay)	"	"
A5	"	"	" (10 sec delay)	"	"
A6	Low	Medium	Yes	600	No
A7	"	"	"	"	Yes
A8	"	"	"	"	" (5 sec delay)
A9	"	"	"	"	" (10 sec delay)
A10	"	Large	"	"	No
A13	"	"	No	"	Yes
C2	H&L	Small	Yes	1200	No
C3	"	"	"	"	Yes
C4	"	"	" (5 sec delay)	"	"
C5	"	"	" (10 sec delay)	"	"
C6	H&L	Medium	Yes	1200	No
C7	"	"	"	"	Yes
C8	"	"	"	"	" (5 sec delay)
C9	"	"	"	"	" (10 sec delay)
C10	"	Large	Yes	1200	No
C11	"	"	" (5 sec delay)	"	Yes
C12	"	"	" (10 sec delay)	"	"
C13	High	"	No	"	"

TABLE II

Variation of Single Vortex Characteristics With Test Parameters

VARIABLES	SMALL NOZZLE	MEDIUM NOZZLE	LARGE NOZZLE
Height (Comparison of high to low position)	Tangential velocity higher with sharper peak. Increase in tangential velocity a maximum of 30%. Increase of Axial velocity of 1 m/sec over entire curve.	Tangential velocity curve at the same height with sharper peak. Axial velocity values consistently 1 m/sec higher.	Tangential velocity curve about the same values except the low position doesn't obtain as sharp a peak. Tangential velocity maximum values 100% higher.
Constant RPM-pressure decay	Decrease in tangential velocity maximum with an increase in corresponding radius. Axial flow steady with a small loss in curve height except for constant axial velocity maximum.	Decrease in tangential velocity maximum with corresponding increase in radius. Axial velocity steady with a slight drop in curve height.	Decrease in tangential velocity maximum with corresponding slight increase in radius. Small steady drop in the Axial velocity curve of 1 to 2 m/sec.
Constant pressure-RPM decay	Tangential velocity maximum decreased with a decrease in corresponding radius. Axial flow steady with a small loss in curve height with little change in Axial velocity maximum.	Tangential velocity decreases with a decrease in corresponding radius. Axial flow steady with a drop in overall curve height.	Due to short period of constant pressure, no trends were indicated.
Increasing nozzle area	The effect of increasing nozzle size was broadening of the tangential velocity peaks while axial velocity curves remained similar with increasing magnitude.		

TABLE III

Dual Vortex Test Parameters

A. Test series I, Medium cage spacing

Contract Test No.	Correlated Test No. 1	Nozzle Size	Cage Rotation		Nozzle Pressure	Cage RPM[2]
			Cage A	Cage B		
2	2MS	Small	Clockwise	Counter Clockwise	Equal	1200
3	3MS	"	"	"	"	600
5	5MS	"	"	"	"	1200
7	7MS	"	"	Clockwise	"	1200
9	9MS	"	"	"	"	600
2	2MM	Medium	Clockwise	Counter Clockwise	Medium	1200
3	3MM	"	"	"	"	600
7	7MM	"	"	Clockwise	"	1200
9	9MM	"	"	"	"	600

TABLE III

Dual Vortex Test Parameters

B. Test series II, Large cage spacing

Contract Test No.	Correlated Test No. 1	Nozzle Size	Cage Rotation		Nozzle Pressure	Cage RPM[2]
			Cage A	Cage B		
2	2LS (2)	Small	Counter Clockwise	Clockwise	Equal	1200
3	3LS	"	"	"	"	600
4	4LS (2)	"	"	"	Plate[3]	1200
5	5LS (2)	"	"	"	Equal	"
6	6L→L (2)	Large/ Small	"	"	"	"
6	6L←L (2)	Small/ Large	"	"	"	"
6	6L→M (2)	Medium/ Small	"	"	"	"
6	6L←M (2)	Small/ Medium	"	"	"	"
5	5ALS	Small	Clockwise	"	"	"
7	7LS (2)	"	"	"	"	"
8	8LS	"	"	"	Plate	"
9	9LS	"	"	"	Equal	600
10	10LS	"	"	"	Plate	"

TABLE III

Dual Vortex Test Parameters

B. Test series II, Large cage spacing (cont.)

Contract Test No.	Correlated Test No.[1]	Nozzle Size	Cage Rotation		Nozzle Pressure	Cage RPM[2]
			Cage A	Cage B		
2	2LM	Medium	Counter-Clockwise	Clockwise	Equal	1200
3	3LM	"	"	"	"	600
4	4LM	"	"	"	Plate	1200
5	5LM	"	"	"	Equal	"
5	5ALM	"	Clockwise	"	"	"
7	7LM	"	"	"	"	"
8	8LM	"	"	"	Plate	"
9	9LM	"	"	"	Equal	600
10	10LM	"	"	"	Plate	"
2	2LL	Large	Counter-Clockwise	Clockwise	Equal	1200
3	3LL	"	"	"	"	600
4	4LL	"	"	"	Plate	1200
5	5LL	"	"	"	"	"
5	5ALL	"	Clockwise	"	None 4	"
7	7LL	"	"	"	Equal	"
8	8LL	"	"	"	Plate	"
9	9LL	"	"	"	Equal	600
10	10LL	"	"	"	Plate	"

TABLE III

Dual Vortex Test Parameters

C. Test series III, Minimum cage spacing

Contract Test No.	Correlated Test No.[1]	Nozzle Size	Cage Rotation		Nozzle Pressure	Cage RPM[2]
			Cage A	Cage B		
2	2SS	Small	Counter-Clockwise	Clockwise	Equal	1200
3	3SS	"	"	"	"	600
4	4SS	"	"	"	Plate[3]	1200
5	5SS	"	"	"	Equal	"
5	5ASS	"	Clockwise	"	"	"
6	6S M	Medium	Counter-Clockwise	"	"	"
6	6S M	Small/Medium	Clockwise	"	"	"
6	6S M	Small/Medium	Counter-Clockwise	"	"	"
6	6S M	Medium/Small	Clockwise	"	"	"
7	7SS	Small	"	"	"	"
8	8SS	"	"	"	Plate	"
9	9SS	"	"	"	Equal	600
10	10SS	"	"	"	Plate	"

TABLE III

Dual Vortex Test Parameters

C. Test series III, Minimum cage spacing (cont.)

Contract Test No.	Correlated Test No.[1]	Nozzle Size	Cage Rotation		Nozzle Pressure	Cage RPM[2]
			Cage A	Cage B		
2	2SM	Medium	Counter-Clockwise	Clockwise	Equal	1200
3	3SM	"	"	"	"	600
4	4SM	"	"	"	Plate	1200
5	5SM	"	"	"	Equal	"
5	5ASM	"	Clockwise	"	"	"
7	7SM	"	"	"	"	"
8	8SM	"	"	"	Plate	"
9	9SM	"	"	"	Equal	600
10	10SM	"	"	"	Plate	"
2	2SL	Large	Counter-Clockwise	Clockwise	Equal	1200
3	3SL	"	"	"	"	600
4	4SL	"	"	"	Plate	1200
5	5SL	Plates[5]	"	"	None[4]	"
5	5ASL	"	Clockwise	"	None	"
7	7SL	Large	"	"	Equal	"
8	8SL	"	"	"	Plate	"
9	9SL	"	"	"	Equal	600
10	10SL	"	"	"	Plate	"

1. These test numbers relate cage spacing and nozzle size to the contract test number.
2. This column indicates the RPM of cage B; cage A was set at 1200 RPM during all tests.
3. For unequal pressures an aluminum plate sealed the nozzle opening at cage B while suction pressure was applied to the nozzle of cage A.

4. Because the cage rotation outlasted the suction pressure available in the vacuum tanks, no suction pressure was applied.
5. Plates were placed across both nozzle openings to improve vortex formation.
6. The cage centerlines were aligned along a north south axis; cage A was to the south of cage B.

TABLE IV

Summary of dual vortex tests

Test		Direction of Cage Rotation		Cage Rotation Speed		Direction of vortex rotation		Number of simultaneous vortices		Total number of simultaneous vortices	Predominate Cage	Unequal Pressure Effect
Series	Spacing	A	B	A	B	A	B	A	B			
I	Medium	C	C	1200	1200	C	C	1 or 2	1	1 or 2	A ——	Not applied
				1200	600	C	0	1	0	1	A ——	" "
II	Large	CC	CC	1200	1200	CC	CC	1	1	1	A ——	Cyclic formation
				1200	600	CC	0	1	0	1	A ——	" "
III	Minimum	CC	CC	1200	1200	CC	CC	1	1	1	No Pref.	Changed cages
				1200	600	CC	CC	1	1	1	No Pref.	" "
I	Medium	C	CC	1200	1200	CC	C	1	1	1 or 2	A ——	Not applied
				1200	600	CC	0	1	0	1	A ——	" "
II	Large	C	CC	1200	1200	CC	C	1	1	2	No Pref.	Pulsed, changed cages
				1200	600	C	0	1 or 2	0	1 or 2	A ——	" "
III	Minimum	C	CC	1200	1200	CC	CC	1	1	1	A ——	Some cage changes
				1200	600	C	C	1	1	1	A ——	" "

Note: Cage rotation speeds are nominal initial speeds.

C Clockwise rotation

CC Counter-clockwise rotation

8. APPENDIX

Dual Vortices

Summaries of selected dual vortices tests are contained herein. The summaries were made from 16mm motion picture recordings of the vortices, tape voice recordings of an observer and the time-history record of pressures and cage rotational speeds.

8.1 TEST: 2LS (2), Contract Test Number 2.

TEST CONDITIONS:

Spacing - maximum
Rotation - counter-rotating
Nozzle opening - small
Pressure - equal
RPM - both cages constant 1178

TEST SUMMARY:

Vortices formed with circulations opposite to the direction of the rotation of their attached cages, Figure 8.1.1. Cores were not always observed with the established vortices. This observed lack of core definition can be attributed to the occasional decrease in density of helium bubbles. In other words, the core was probably present whenever a vortex was formed; however, helium bubbles were not always available to fill the core.

During three runs, two vortices formed simultaneously at both cages on three occasions. Cores were observed present in both of the vortices on two of these occasions.

Core bases roamed particular zones on the false floor throughout all three runs. The zone for cage A was approximately 30 cms from the cage center toward cage B. The zone for cage B was approximately 30 cms from the cage center toward cage A. Each zone covered an area of about .4m^2. (Note: In run number 3, the core base of the vortex attached to the cage B did travel momentarily to the right of the center of cage B).

Vortices were observed to disappear intermittently, but usually reformed quickly. Cores were also observed to disperse occasionally

when the core head was detached from a cage. Prior to dispersing, the core would hang, then fall, then ascend, then fall again. These undulations would last for two to three cycles before the core finally dispersed by spinning-out.

8.2 TEST: 3LS, Contract Test Number 3.

TEST CONDITIONS:

Spacing - maximum
Rotation - counter-rotating
Nozzle opening - small
Pressure - equal
RPM - constant 1198 at the south cage and 600 at the north

TEST SUMMARY:

Cage A appeared dominant, Figures 8.2.1 and 8.2.2. Vortices with circulations corresponding to cage A rotation formed at cage A prior to the application of pressure. After the application of pressure, the vortices appeared to favor the region in between cages. The core base wandered back and forth between positions under cage A and in between cages while the corehead would whip back and forth from the cage A to a position in between the cages. The core head occasionally reached cage B but never attached to cage B even though the core base traveled to a position beneath cage B.

The following are some unusual occurrences observed during the three runs:

1. Two vortices formed simultaneously; one beneath cage A and one in between cages. Both had circulations corresponding to cage A rotation. The vortex in between cages merged with the general

circulation. The vortex beneath cage A became the established vortex and traveled in between cages. The core velocity was of a low magnitude and the core base traveled beneath cage B. The core fell to a 120 cm height, hung, then stretched upward and attached to the south cage.

2. The core head detached from cage A while the core base was in between cages. The core head occasionally reached the framework and violently whipped about. The core fell to a 120 cm height, hung, ascended back to the framework and hung suspended. The core head fell back to a 120 cm height and again hung. This cycle was repeated several times before the core head reattached to cage A.

8.3 TEST: 8LS, Contract Test Number 8.

TEST CONDITIONS:

Spacing - maximum
Rotation - corotating
Nozzle opening - small
Pressure - unequal (plate covers north nozzle opening)
RPM - decaying

TEST SUMMARY:

Vortices formed with directions of circulation corresponding to the direction of cage rotation, Figures 8.3.1 and 8.3.2. General room circulation also corresponded to cage rotation. Vortices formed predominantly on cage A, but often attempted to transfer to cage B with an occasional success. These attempts to transfer were indicated by the frequent movement of the core base in between cages with the core head still attached to the outside of cage A. At times, with the core base in this location, the core head would move back and

forth from inside cage A to the outside of the cage. Also, with the core base in this position, the core head was observed to frantically switch back and forth between cage A and cage B for a short period of time.

Throughout all runs, vortices displayed cyclic vortex formation. Average core and vortex life was 1 to 5 sec. Normally the core would dissipate, with the vortex surface still present, and quickly reform. The core dissipated when the head detached, core flow ceased, the core fell and the vortex surface velocities caused the core to spin-out. During dissipation, vertical velocities at the vortex surface were zero while tangential velocities were slow to moderately fast. Occasionally, prior to spinning out, the core would assume a wavy shape and whip about beneath the cages. Rarely, the vortex surface would dissipate when the core dissipated, but usually it quickly reformed.

Normally, vortices favored cage A or sink. If vortices transferred to cage B, they did so after the negative applied pressure was nearly depleted and remained for only a short period of time.

8.4 TEST: 3SL, Contract Test Number 3.

TEST CONDITIONS:

Spacing - minimum
Rotation - counterrotating
Nozzle opening - large
Pressure - equal
RPM - constant 1198 at cage A and 600 at cage B

TEST SUMMARY:

At the beginning of each run, negative pressure was applied with a vortex and core attached to cage A, Figure 8.4.1. Circulations of all vortices during the test corresponded to the rotation of cage A. Vortex/core systems were observed attached to cage B three times during the test: Once prior to application of pressure and once after the pressure had depleted (during the same run) and once shortly after pressure was applied (during a different run). Vortices "tightened-up" after the application of pressure and velocities remained large in magnitude until the end of the run.

Prior to pressure during the start of one run, the vortex core, attached to cage B, fell to a height of 120 cm. Hanging momentarily, the core then ascended to attach to the outside of cage A and finally moved to the inside of the cage. The vortex remained at cage A until the pressure had diminished and then returned to cage B.

8.5 TEST: 9SL, Contract Test Number 9.

TEST CONDITIONS:

Spacing - minimum
Rotation - corotating
Nozzle opening - large
Pressure - equal
RPM - constant 1198 at cage A and constant 600 at cage B

TEST SUMMARY:

At the beginning of each run a vortex formed usually with a circulation corresponding to cage rotation. During two runs the vortex survived almost until the end of the run before dissipating. In the other run the vortex did last throughout the entire run. In all runs, numerous small vortices with circulations opposite to cage rotation were observed to intermingle and spin-off the existing vortices. Vortices, in general, did appear to favor cage A and travel away from the observer when leaving either cage.

Prior to application of negative pressure in one run, a cycle of building and dissipating vortices was observed. A vortex with a circulation opposite to cage rotation would first form at cage B, Figure 8.5.1. The core base would travel from its initial position, 30 cm northwest of cage B, to the northwest edge of the platform while the core head remained attached to cage B. When reaching the floor edge the vortex dissipated. At the same time B vortex dissipated, another vortex with a circulation that corresponded to cage rotation would build to the left of cage A and travel to the right to attach to cage A. The core base would continue to travel northwest to a position in between cages and close to the floor edge where it would dissipate.

The formation and dissipation of these two vortices completed one cycle; for, as A vortex dissipated, the B vortex would build again beneath cage B.

In the last run, vortices formed and behaved inconsistently with those observed in the first two runs. Some were observed to form and travel away from,while others traveled to the left.

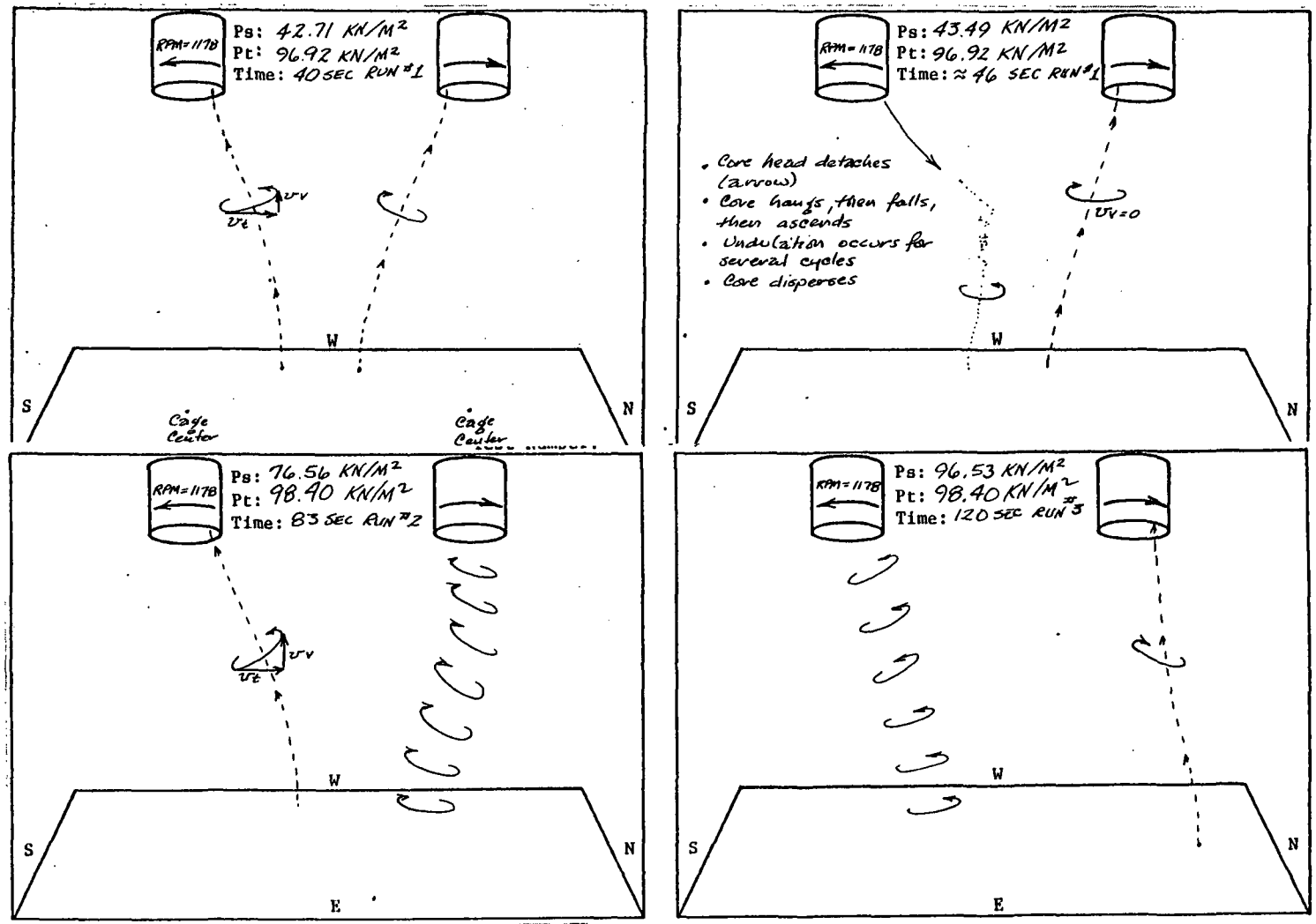

8.1.1 Dual vortices formed by counter-rotating cages of equal speed with maximum spacing and equal pressures.

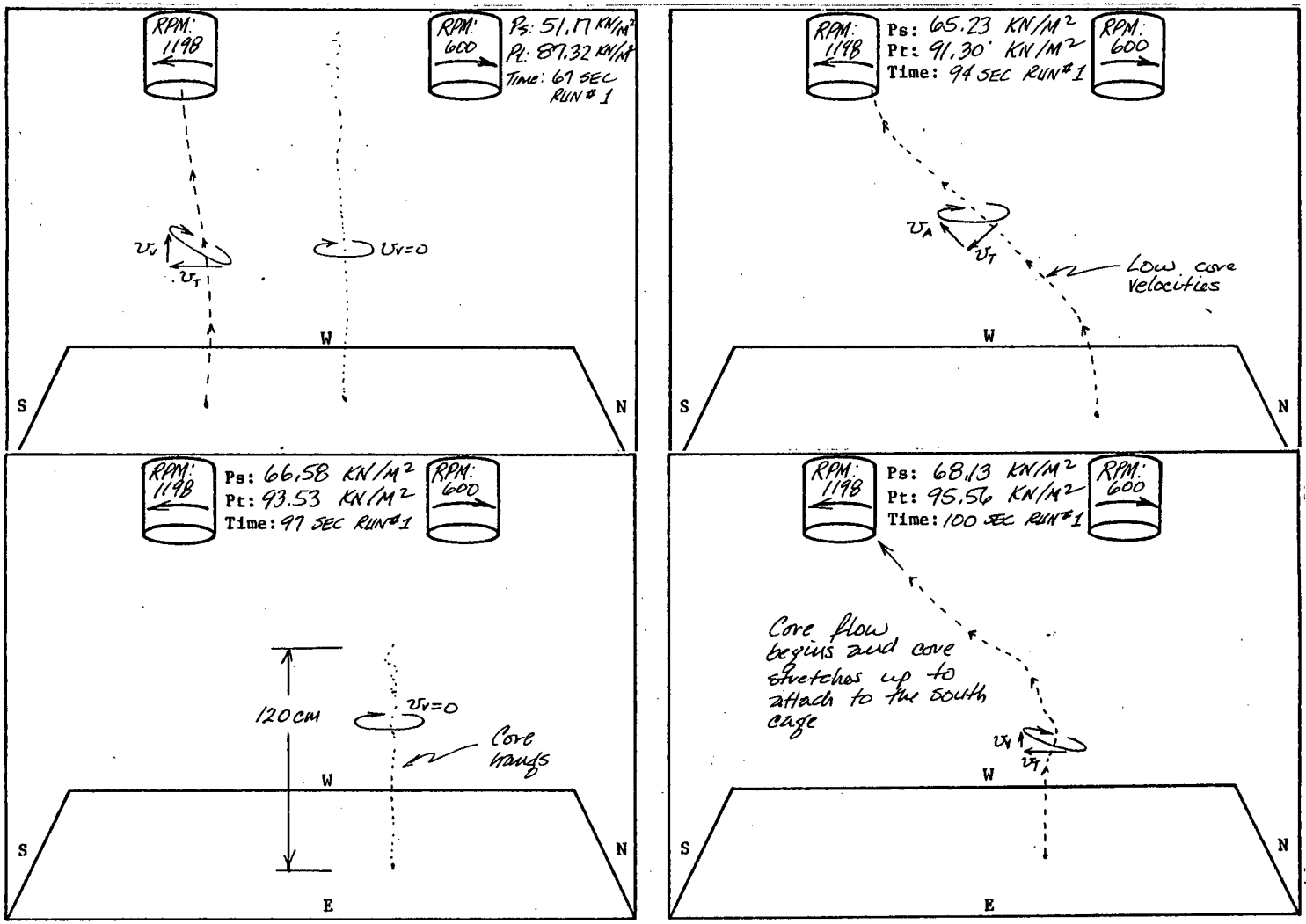

8.2.1 Dual vortices formed by counter-rotating cages of unequal speed with maximum spacing and equal pressures.

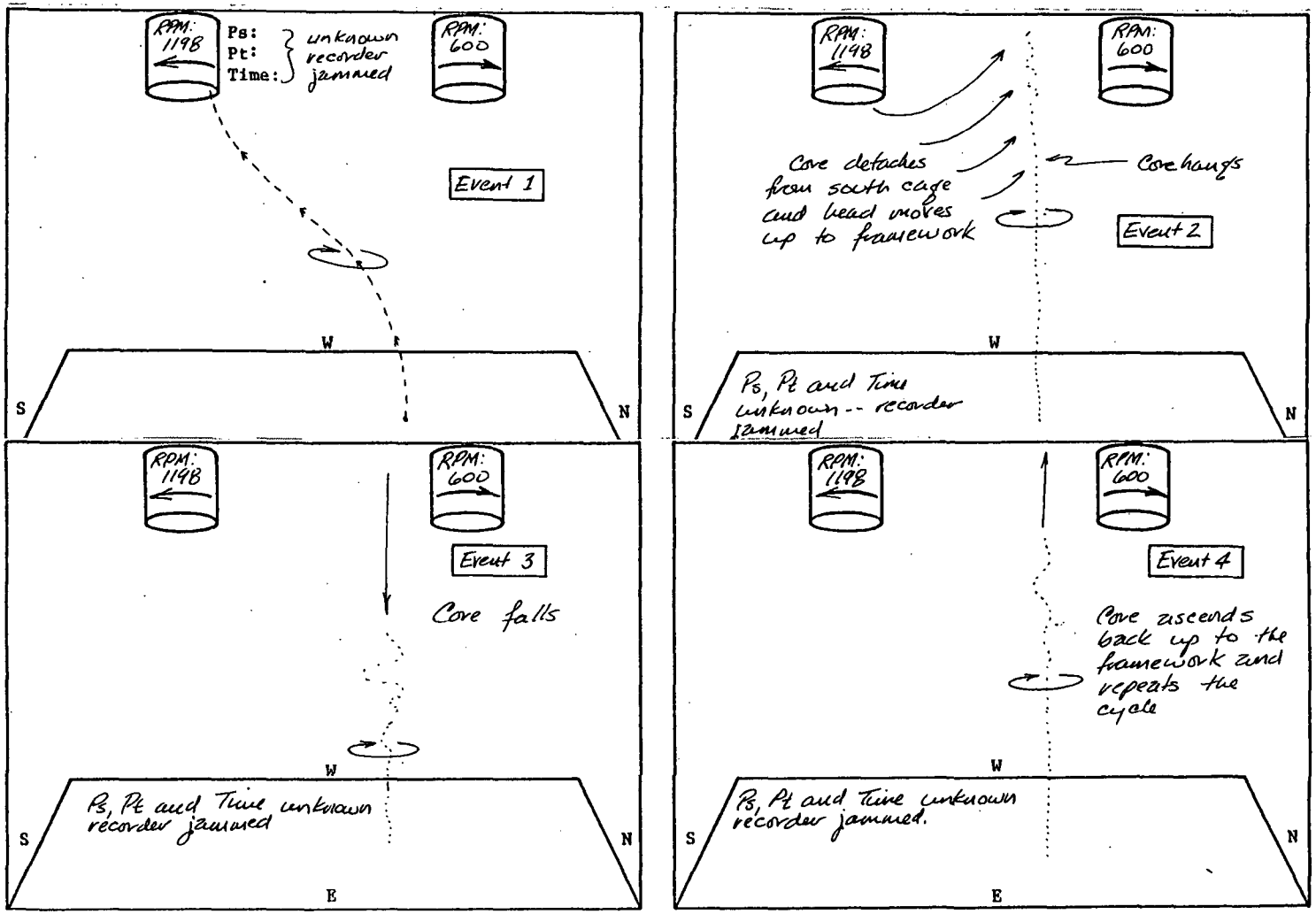

8.2.2 Single vortex formed by counter-rotating cages of unequal speed with maximum spacing and equal pressures.

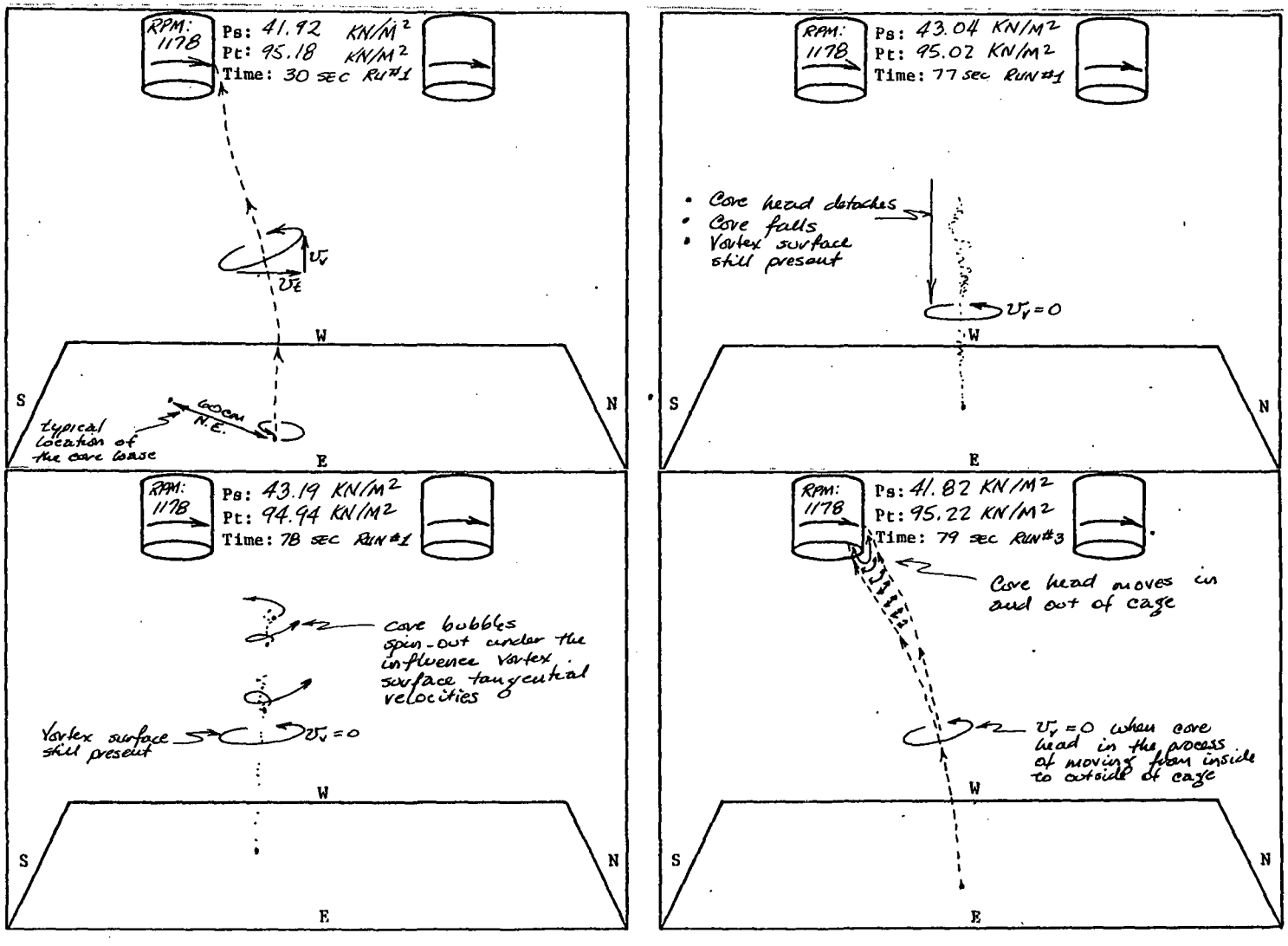

8.3.1 Cyclic formation and blow-out of single vortex formed by corotating cages of equal speed with maximum spacing and unequal pressures.

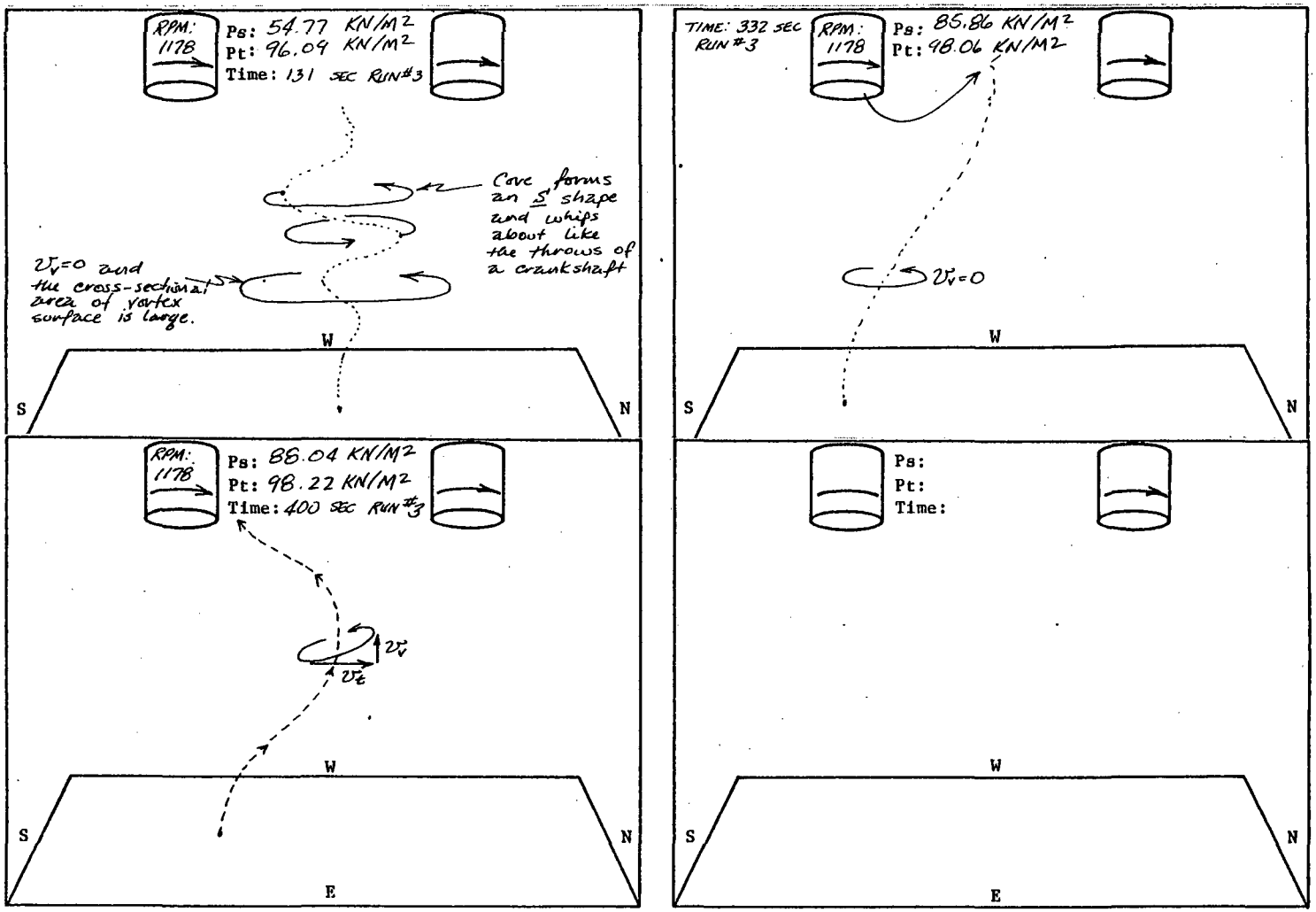

8.3.2 Cyclic formation and core "whipping" of single vortex formed by corotating cages of equal speed with maximum spacing and unequal pressures.

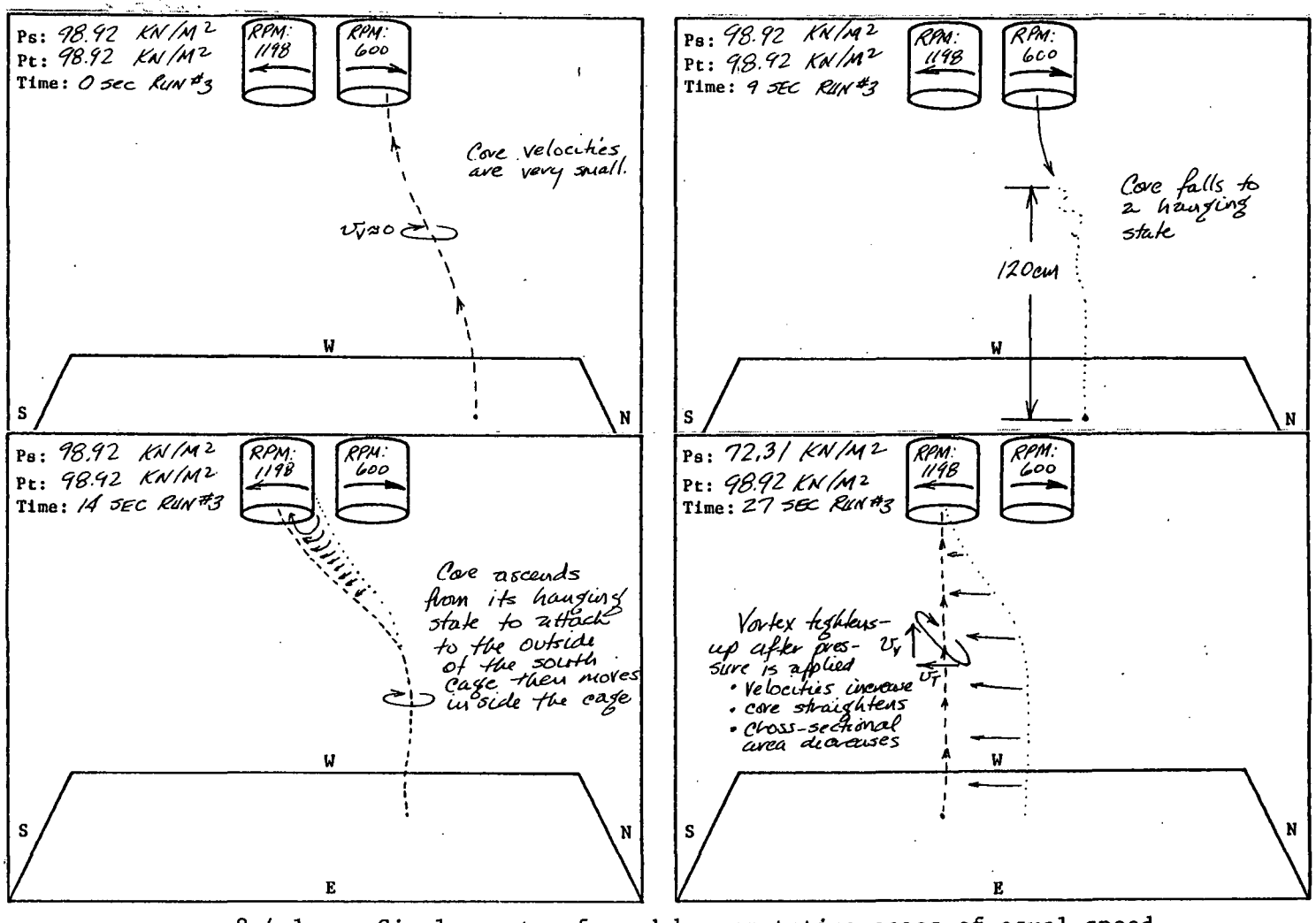

8.4.1 Single vortex formed by corotating cages of equal speed with minimum spacing and equal pressures.

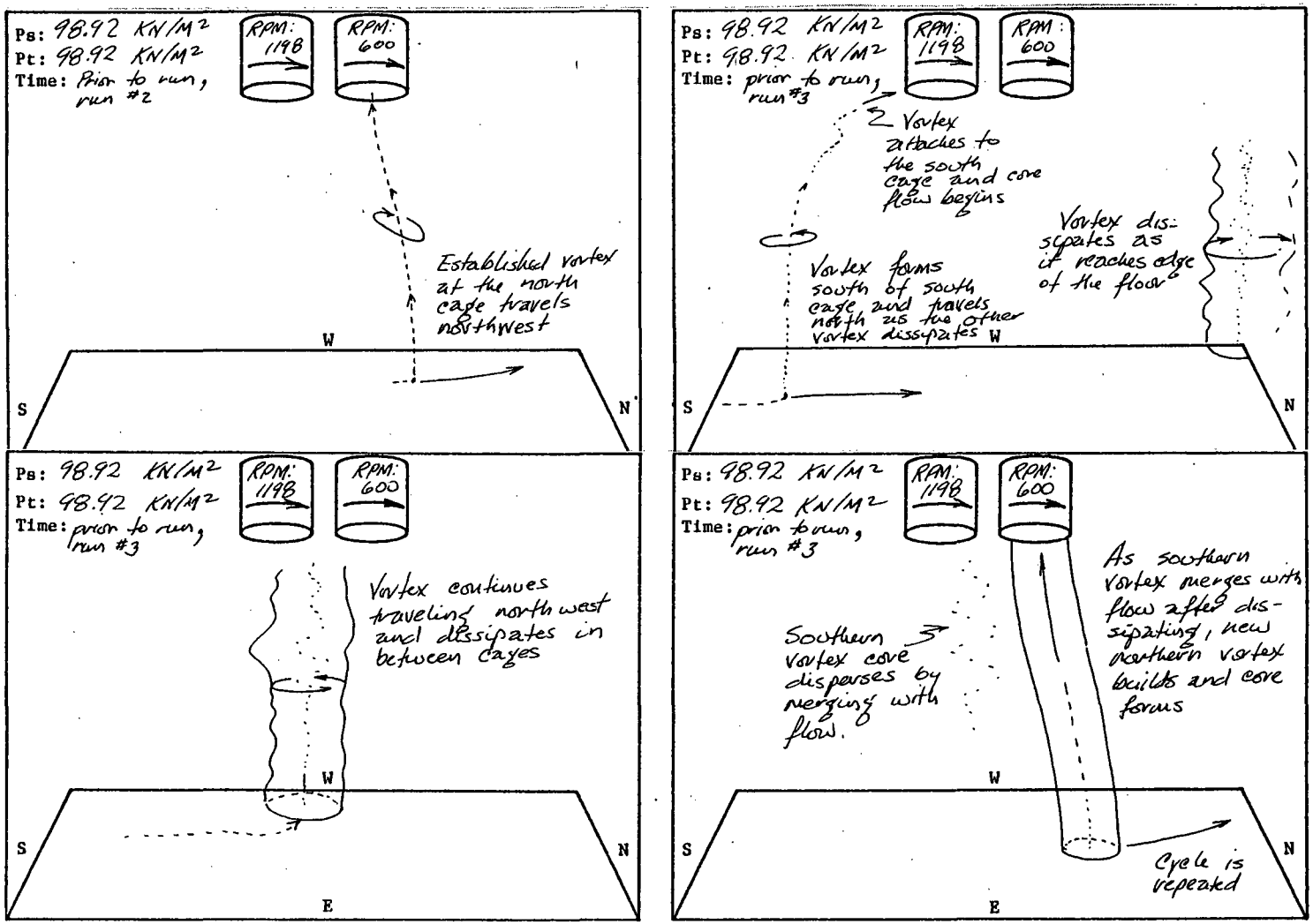

8.5.1 Cyclic formation - single vortex formed by corotating cages of unequal speed with minimum spacing and equal pressures.